Article

Not peer-reviewed version

Comparison of Melting-Affected Rocks from Presumed Small Impact Craters and Old Limekilns in Bavaria, Germany

Václav Procházka , Horst Herrmann , Pavel Kalenda , Petr Martinec , Jiří Mizera * , Tomáš Trojek , Lenka Thinová , Gunther Kletetschka , Jan Adámek , Kamil Souček

Posted Date: 22 March 2024

doi: 10.20944/preprints202403.1373.v1

Keywords: limekiln; impact crater; glass formation; thermoplastic deformation

Article

Comparison of Melting-Affected Rocks from Presumed Small Impact Craters and Old Limekilns in Bavaria, Germany

Václav Procházka [1], Horst Herrmann [2], Pavel Kalenda [3], Petr Martinec [4], Jiří Mizera [5,*], Tomáš Trojek [1], Lenka Thinová [1], Günther Kletetschka [6,7], Jan Adámek [1] and Kamil Souček [4]

[1] Faculty of Nuclear Sciences and Physical Engineering, Czech Technical University in Prague, Břehová 7, Praha 1, 11519, Czech Republic; vaclav.prochazka@fjfi.cvut.cz (V.P.); tomas.trojek@fjfi.cvut.cz (T.T.); lenka.thinova@fjfi.cvut.cz (L.T.); jan.adamek@fjfi.cvut.cz (J.A.)
[2] Zugspitzstraβe 11, Bernried am Stanberger See, 82347, Germany; herrmann-bernried@t-online.de
[3] CoalExp, Pražmo 129, 73904 Czech Republic; p.kalenda@volny.cz
[4] Czech Academy of Sciences, Institute of Geonics, Studentská 1768, Ostrava-Poruba, 70800, Czech Republic; martinec@ugn.cas.cz (P.M.); kamil.soucek@ugn.cas.cz (K.S.)
[5] Czech Academy of Sciences, Nuclear Physics Institute, Husinec-Řež 130, 25068, Czech Republic
[6] Faculty of Science, Charles University in Prague, Albertov 6, Praha 2, 12843, Czech Republic; gunther.kletetschka@natur.cuni.cz
[7] Geophysical Institute, University of Alaska-Fairbanks, 2156 N Koyukuk Drive, Fairbanks, AK 99775, USA
* Correspondence: mizera@ujf.cas.cz

Abstract: Depressions containing partially molten rocks were investigated in Quaternary pebbly sediments in Alpine foreland in Bavaria, Germany. Ruins of limekilns from 18-19th centuries are abundant around Seeshaupt. They are usually associated with earthworks for fuel feeding and protection from wind. Depressions contain partially molten stones from furnace walls, with lime and burnt loam remnants. On the surface of pebbles (typically gneisses), green glass formed with chemical composition possibly affected by moderately volatile components of wood biomass, mainly K and Cu. Thermoplastic deformation of pebbles is limited and the surface melt deformation points to slow flow. At Emmerting, on the other hand, two walled circular depressions which lack additional earthworks have been identified as possible impact craters. Thermally affected pebbles show much more intense deformation. Colorless to greenish glass, also K and Cu enriched, usually forms only thin surface coatings, in places covered by younger melt extruded from pebble interior. Burnt loam is missing. At Grabenstätt-Kaltenbach, a depression of unclear origin was investigated. Morphologically, it matches craters rather than limekilns, but anthropogenic contamination (brick-like material) is probable. The rare molten samples do not display extreme deformation features. The thermally affected stones, mainly those from Emmerting, have elevated magnetic susceptibility.

Keywords: limekiln; impact crater; glass formation; thermoplastic deformation

1. Introduction

The production of lime has been of key importance for architecture. In the peak Middle Ages and early modern history, lime was relatively expensive in Central Europe, being usually produced in sophisticated and specialized limekilns (e.g., [1]). Starting approximately in the 18th century, the rural consumption of lime mortar increased and the local lime production (in regions with raw material available) became common, characterized by usage of many small furnaces. Primitive lime burning exists in less industrialized countries or regions.

Relics of old limekilns can be tracked down by earthworks, reaction products of lime or imperfectly burnt carbonate, and potentially various other thermally affected materials including silicate rocks. However, when historical documentation as well as unequivocal artifacts are missing,

 doi:10.20944/preprints202403.1373.v1

such objects may present a complicated task for geologists and archaeologists, as they may have formed in various other ways – natural (including meteorite impact) as well as anthropogenic (e.g., metallurgy, wood charcoal production, and various constructions affected by intentional fire or wildfire).

Here we document similarities and differences between several ruins of limekilns, two small impact craters, and one structure of uncertain origin. All objects have been found in similar environment (forested areas in southern Bavaria, Germany; see Figure 1) with similar geological background, dominated by coarse pebbles which represent both carbonate and silicate rocks, including sandstones and quartzites.

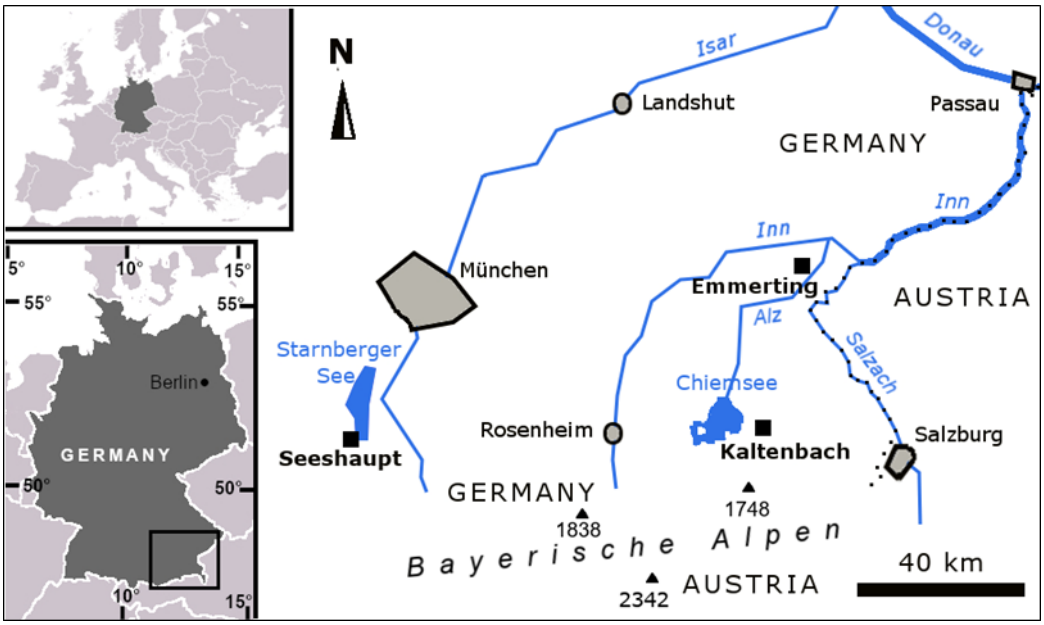

Figure 1. Map with the localities and areas investigated (squares).

1.1. Limekilns in the Surroundings of Seeshaupt

The collection of one of the authors (H. Herrmann) comprises more than 130 samples from 23 locations mainly in the estates of the town Seeshaupt and commune Eberfing, west of the southern edge of the Starnberger See lake (see also [2]). Basic characterization of the limekilns has largely been adopted from the report [2]. Almost all kilns are located on a hillslope, with a furrow for fuel feeding oriented downwards. Other earthworks are frequent, mainly banks/mounds for thermal isolation and perhaps to funnel the air flow. Thermally affected stones are concentrated in the upper depression and its walls (occasionally on a bank at the downhill side). This circular or elliptical depression has 2–4 m in diameter and it is virtually a ruin of the shaft furnace which was probably a 3–4 m high blunted cone (by analogy with depicted field kilns in Vienna surroundings from the end of 18th century [2]). Many of the kilns are in historical maps [3]. The oldest maps from the Seeshaupt area are from years 1809-1810. Some limekilns are mentioned in historical documents since 1739 (Frechensee); see [2] for details.

Geological background consists of coarse Quaternary sediments, namely fluvial terraces and moraines (formed by the Isar-Loisach Glacier), which is typical for the Alpine foreland [4]. The sediments are unconsolidated, which made it possible to collect limestone as well as other rocks for construction of the kiln from cultivated fields. Sintering and partial melting of kiln walls implies temperatures achieved by wood combustion in excess of 1000 °C, although temperatures over ca. 900 °C decrease porosity and reactivity of the produced quicklime [5]. The initial overburning may have been aimed at strengthening the construction, or the higher temperatures were unintentional.

1.2. Craters at Emmerting and Potential Crater at Grabenstätt-Kaltenbach

 doi:10.20944/preprints202403.1373.v1

Several depressions in west to north surroundings of Burghausen were suggested to be small impact craters [6–8]. Most of them formed in coarse unconsolidated Quaternary sediments, namely fluvial terraces and moraines. Impact craters in such soft target materials often lack signs of shock metamorphism as a standard criterion for impact confirmation, and most such craters have only been confirmed thanks to findings of iron meteorite fragments [9].

The structure No. 4 at Emmerting (for numbering, see [7,8]) has been investigated as the most promising one, and it has been shown that there is no viable alternative to impact [8,10]. Recently a stone (enstatite-rich) meteorite fragment has been found in the crater filling [11,12] together with more particles likely formed by melting of the same body. Characterization of the meteoritic material is presented in our companion paper [13], together with hollow spheroid Fe-oxide particles, potentially formed by impact.

The nearby Crater No. 5 was probably influenced by inundations from side channels of the Alz river. Both craters are out of reach of last glaciation and cannot be interpreted as glacial kettle holes. The closest young moraines of the Salzach Glacier from Alps are located ca. 10 km to the south [14]; moreover, the Crater No. 5 formed in a Holocene terrace [4]. Other natural processes which could form such depressions, like volcanism, methane explosions or salt leaching, can be excluded in Quaternary sediments in the region (see [3,4)]. Similarly, other natural processes which can produce glasses, like underground fires, frictional melting on fault- or rockslide planes or lightning [15], are irrelevant due to regional geology, and/or unable to explain melting of large pebbles or their nearly whole surfaces. The geophysical results are consistent with impact origin of the craters, indicating among others compact bodies below their bottoms [10,11,16].

Finally, we analyzed a circular depression with high-temperature effects at Grabenstätt-Kaltenbach which was also investigated as a potential impact crater ([17] and references therein). As the Emmerting craters, it is located in the so-called Chiemgau Impact strewn field which, according to the proponents, contains more than 100 craters (with up to 1 km in size) of Holocene age, formed most likely in the 1st millennium BC, perhaps at the end of the Bronze Age [6,8,18,19]. The strewn field would form an ellipse elongated from northeast to southwest. The Chiemgau Impact theory, however, is highly controversial, as shown mainly in the discussions about the origin of the lake Tüttensee (near Grabenstätt) and a potential impact into the Lake Chiemsee (see [20–22] and references therein). Nevertheless, the discussion of relatively large, water-filled or buried potential impact craters in the region, as well as discussion of the whole Chiemgau Impact theory is beyond the scope of our paper. We concentrate on melting and deformation of pebbles in comparison with thermally affected stones from limekilns.

2. Site and Sampling Description

2.1. Limekilns

Samples were collected from depths not exceeding 20 cm not minimize disturbing potential future archaeologic research; they were mostly hidden below leaf litter or humus. The material remained from the kilns includes mainly silicate rocks from collapsed walls, and relics of lime and of burnt loam, which may have imprints of spruce twigs. Six samples were documented microscopically. Magnetic susceptibility (MS) was measured in 20 samples and elemental composition determined in 18 samples. The samples presented here come from 7 limekilns. An example of a limekiln is shown in Figure A1.

2.2. Emmerting: Crater No. 4

A walled crater with a diameter of the depression ca. 8 m and a diameter including walls up to 13 m (Figure A2) is located ca. 1.5 km north of the center of the Emmerting town (48.21278N, 12.7706E, 410 m a.s.l.) on a mild southeast slope in a beech forest; the wall was cut by a trench for scientific purposes on the southern side. The crater was formed in Quaternary river terrace with typical pebbles from Alps, including sediments (prevalently limestone – carbonate rocks form about a half of pebbles in the area) as well as crystalline rocks (quartzites, gneisses, amphibolites, and plutonic rocks). The

 doi:10.20944/preprints202403.1373.v1

terrace is the second one from the recent Alz river upwards (Niederterasse) whose age is Late Glacial (12 -15 ka) [4]. At least 100 years old trees grow from the crater walls and floor [10].

Strong high-temperature metamorphism, thermoplastic deformation and possibly volatilization were documented in [10,23]. Melting was selective and little affected quartz even in rocks where eutectic melting of quartz should take place. Moreover, extreme fracturing of mineral grains and indices for shock metamorphism (prevalently from petrographic microscope only) were presented: possible planar deformation features (PDF) of several directions in quartz and feldspar, diaplectic quartz, and spalling [23]. High-temperature effects are mainly observed in cobbles and pebbles or their fragments having ≥ 4 cm in size. The fine-grained fraction of the filling mostly represents thermally unaffected material which has been deposited after crater formation, when the original fine-grained material was largely volatilized or mechanically removed [12,13]. Pebbles welded together with a silicate melt occur in the crater as well as in the wall, showing that and high temperature persisted for some time after its formation [8,10], perhaps due to fire of remaining biomass.

Some authors [10,23] claimed lack of carbonate pebbles in the crater as compared to the surroundings. In the crater floor as well as in the inner part of the wall (as documented in the trench), numerous sharp-edged crushed limestone fragments can be found (similar to other small crater-like structures in the area [6]) which are sometimes sintered together. This could be explained by disintegration of relatively soft carbonate pebbles during crater formation.

2.3. Emmerting: Crater No. 5

A walled crater with a diameter of the depression ca. 8 m, a diameter including walls up to 12 m and a depth 1–1.2 m (Figure A3) is located ca. 2 km north-northeast of the center of the town Emmerting (48.2179° N,12.7803° E, 390 m a.s.l.) in a mixed forest. The target sediments rich in coarse pebbles belong to the lowest terrace which is elevated 3 m above the recent alluvium plane of the Alz river. The terrace age is Holocene [4]. Pebbles with visible melting are much less abundant than in Crater No. 4. Yellow sediment identified as marl could represent a younger autochthonous filling.

2.4. Depression at Grabenstätt-Kaltenbach (the Kaltenbach Structure)

A walled structure with 7–8 m diameter including walls is located at the summit of a forested moraine ridge near its eastern slope, 2 km east of the Chiemsee lake at the town Grabenstätt, west of the settlement Kaltenbach (47.8695° N, 12.5580° E, 575 m a.s.l.; Figure A4). Ernstson [19] reported a morphology well corresponding to an impact crater prior to recent investigation.

According to trees, the structure should not be younger than a century. Most rock samples are fragments of originally rounded, commonly up to 30 cm-sized limestone pebbles. Samples of gneiss and quartzite with notable glass coatings were selectively collected for research (e.g., [17]), but limestone pebbles prevail in the surroundings as well. Also, angular sandstone cobbles occur. The central part of the depression was recently excavated by digging (Figure A4).

High MS of the subsoil in the crater and the close surroundings was documented [8,24], forming a circle of ca. 15 m in diameter with MS up to one order of magnitude higher. Also cobbles of various rocks from the crater have elevated MS and usually even significant remanent magnetization. Neumair et al. [17] documented partially molten rocks in the form of cobbles and sharp-edged fragments from 20–50 cm depths.

2.5. Sampling at Emmerting and Kaltenbach

In 2015, we collected and catalogued 25 samples in the Kaltenbach structure (#101–125) out of which 21 are whole pebbles or large fragments, and 23 pebbles in Crater No. 4 at Emmerting (samples #401–422 and #15240). Samples were taken from shallow depths (in the order of decimeters) from the soil within the craters. No exact position was noted because the material had been dug up several times. Nevertheless, filling of fractures with soil and fine penetration of roots through many pebbles exclude that they could be brought to the sites recently (see also 4.3.1).

 doi:10.20944/preprints202403.1373.v1

In 2016, we collected and catalogued the samples #16129–16133 and in addition, samples at profiles in Crater No. 4 were taken (from 6 spots with 1–5 samples in each spot). Several samples were chipped off the glass-rich area near the original crater floor. No correlation of the occurrence of high-temperature or deformation effects with their locations in profiles was found. Nevertheless, sample numbers referring to their position in profiles are preserved, e.g. 4/1/–3 means: Crater No. 4 / Profile 1 / –3 m. The samples 5/1/0a,b were collected from the center of Crater No. 5 (see also [16] for exact profile positions).

3. Analytical Methods

Minimally invasive methods were preferred. Field measurements with several geophysical methods were also performed at Emmerting. Here we present only results of gamma-ray spectrometry as a first order indicator of quantitative geochemistry. For the results of ground-penetrating radar, automatic resistivity system, and radon measurements, see [16]. A binocular stereomicroscope was used for observation and photographing surfaces of original samples, as well as of those cut or partially broken. Surface glasses were analyzed mainly by X-ray fluorescence. Thin sections were prepared from selected samples and investigated with a petrographic microscope and a scanning electron microscope.

3.1. Field Gamma-Ray Spectrometry

In situ measurements of concentrations of K, U, Th and ^{137}Cs were performed mainly in five profiles over Crater No. 4 and Crater No. 5. The depth range of this method is usually 35-50 cm. A portable GT40 spectrometer (Georadis, Brno) with a 3×3" NaI(Tl) detector was used. The spectrum up to 3 MeV is stabilized using gamma energies of natural radionuclides. In addition, 10 points in the Kaltenbach structure and surroundings were measured with a GT30 instrument (^{137}Cs was not quantified). The spectrometers were calibrated and verified in the calibration base in Bratkovice, Czech Republic, for measurement in 2π geometry. The sampling time was set to 3 minutes at each spot.

3.2. Magnetic Susceptibility (MS)

Laboratory determination of bulk susceptibility was carried out with an SM-30 instrument (Z.H. Instruments, Brno). Exact measurement is possible for samples of 2×2×2 cm in size or larger.

3.3. X-ray Fluorescence (XRF)

Elements heavier than Mg were semiquantitatively determined on flat glass surfaces and unpolished sections by a Delta Premium XRF analyzer. The analytical mode 'Geochemistry' with a spot diameter 10 mm (if necessary, 2 mm only), two beams with voltage 50 kV and 10 kV, and fully automatic interpretation of spectra were used. Samples from lime kilns and a few samples from craters were analyzed at similar conditions (always with 10 mm beam size) with a portable VANTA instrument.

Measurements of individual phases were mainly performed with a XRF analyzer consisting of a Mini-X X-ray tube (35 kV, 10-90 μA) and SDD detector. The beam diameter of the analyzed area was set approximately between 1 and 3 mm, with lateral resolution down to 0.4 mm.

3.4. Scanning Electron Microscopy (SEM), Electron Microprobe (EMP)

In addition to thin-sections, we also used (especially for surface coatings) samples with uneven surfaces, where full quantitative microanalysis was impossible. An electron microscope with a microprobe with energy-dispersive analytical system (EDS), mostly a TESCAN Vega instrument with X-Max 50 detector, was used, also for back-scattered electron (BSE) and secondary electron (SE) imaging. Detailed BSE images were also obtained with a JEOL JSM-5500 instrument.

3.5. Computer Tomography (CT)

 doi:10.20944/preprints202403.1373.v1

An X-Ray computer tomograph Nikon XTH 225 ST was used. The CT Pro 3D software was used for processing of radiographic images. CT volume and tomographic slices were evaluated by the VGStudio Max software (versions 2.2 and 3.3.2).

3.6. Determination of Glass Melting Temperature

Standardized pyrometric tests (ČSN ISO 540) with small pieces of glass-dominated re-melted rock were performed. A sample from Crater No. 4 was tested at the Institute of Geonics, Ostrava. It was heated in reducing and oxidizing atmospheres up to 1500 °C, with a 50 °C step and 30 min duration of each temperature. Samples from limekilns were tested in a similar way at the Geochemical Institute of the Frankfurt University and at the Bavarian Geological Institute in München.

4. Results and Discussion

4.1. Field Gamma-Ray Spectrometry

Contents of K, Th and U obtained from the field gamma-ray spectrometry are presented in Table 1. Compared to the continental crust composition, concentrations of K, Th and U are very low, low, and low to average, respectively, reflecting composition of the pebbles forming the bedrock: high amount of limestone, calcareous sandstone and quartzite, low amount of granitic rocks, and absence of alkaline igneous rocks or their metamorphic equivalents in the terrace sediments. The geological background cannot explain the enrichment of glass in K. In addition, both profiles crossing Crater No. 4 show minima of radionuclides in its center (perhaps due to low clay and silt contents) and maxima of K (also Th in one case) in its walls. Similarly, the Kaltenbach structure is somewhat depleted in K and Th (including low Th/U ratios) in comparison with the surroundings (Table 1).

Table 1. Contents of K, Th and U obtained from the field gamma-ray spectrometry (mean values from *n* measurements, K in wt.%, equivalent Th and equivalent U in ppm, ^{137}Cs in kBq/m^2).

Location	Object	*n*	K	eTh	eU	Th/U	^{137}Cs
Eichendorf	limekiln 6 (Tradfranz 1)	1	0.33	1.88	2.52	0.75	4.86
(Eberfing)	limekiln 22 (Eichendorf)	1	0.55	2.75	2.53	1.09	7.80
Emmerting	Crater No. 4 and surroundings	90	0.60	4.75	2.17	2.19	5.18
	Crater No. 5 and surroundings	62	0.50	2.50	1.50	1.67	5.84
	Niederterasse far from craters	3	0.55	4.43	2.41	1.84	5.47
Kaltenbach	depression	4	0.56	4.13	2.68	1.54	n.a.
(Grabenstätt)	surroundings	6	0.74	5.57	2.90	1.93	n.a.

4.2. Petrography and In Situ Transformations - Limekilns

4.2.1. Structural and Textural Characteristics

The dominant rock type of the glass-coated stones is gneiss with the foliation visible particularly on biotite crystals. The surface glass is usually colorless to green, rarely very dark to black, or transitional yellow-brown; various blue tones (bluish to turquoise) are common which resemble Cu^{II}–bearing secondary minerals and are possibly influenced by Cu content in glass. In typical gneiss samples, glasses derived from biotite (black, with open pores; Figure 2A) and from feldspars (colorless) can be distinguished. Macroscopically white melt usually contains relics of quartz, secondary SiO_2 phases, or abundant bubbles. In mafic or calcite-rich rocks, relatively homogenous but porous melt (with grey, brown or other color) may form (Figure 2B,C), in some cases with relics of quartz. Transition between partially or fully melted rock interior and surface glass can be gradual,

 doi:10.20944/preprints202403.1373.v1

with glass of various colors partly following the original bands of various minerals. In other cases, glass (especially the green one) forms a clearly delimited and partly "peeling-off" layer covering sandstones or gneisses (Figure 3). White relics of lime on the surface are abundant; they may have influenced the surrounding melt by mixing (causing brightening of the green glass, e.g.).

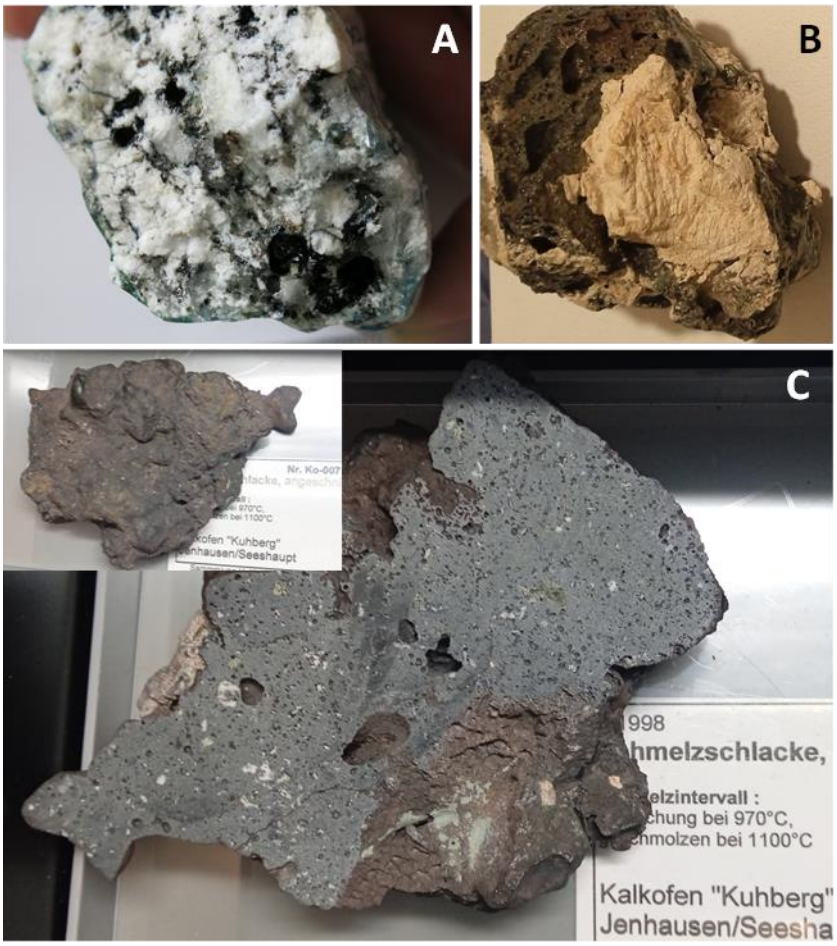

Figure 2. (**A**) Gneiss with expanded biotite (dark) (Ko-110, Tradfranz 1; image width 6.5 cm). (**B**) Highly porous "slag" – re-melted intermediate (slightly mafic) rock with relics of lime on the fracture and locally (right bottom) with green surface glass (Ko-081, Wolfetsried; image width 7 cm). (**C**) Re-melted basic rock (amphibolite?), also used for melting test (Ko-007, Kuhberg; image width 16.5 cm; rear view inserted).

Figure 3. (**A**) Calcareous sandstone with thick, usually dark green glass, in places contaminated with a bright earth or lime (Ko-003, Kohlstatt). (**B**) Partial peeling-off of the greenish glass from a gneiss

 doi:10.20944/preprints202403.1373.v1

pebble's surface; the dark bands formed by melting of biotite; image width 11.7 mm (Ko-087, Kuhberg).

The glass may contain newly crystallized minerals, especially near the surface. An example is shown in Figure 4, namely snowflake-like aggregates, typical for tridymite [25]. Other colorless crystals, usually forming clusters, spherolites or network-like aggregates, cannot be identified in stereomicroscope, but they could include mainly acicular plagioclase, diopside, devitrite, cristobalite, and others; the proximity to the surface suggests that local volatile loss of alkalis lead to the crystallization (see [25]).

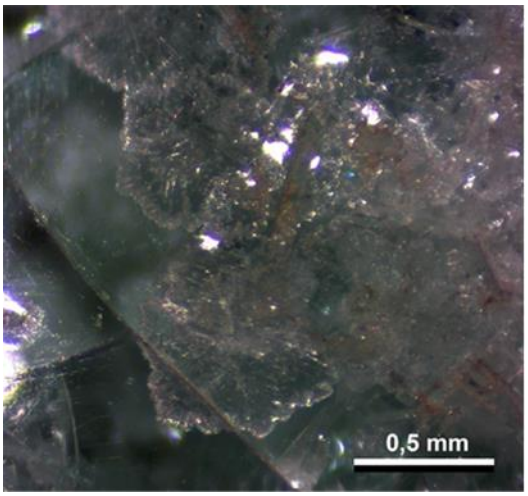

Figure 4. Typical snowflake-like aggregates of tridymite very close to the glass surface (Ko-087).

Deformations of melts have been observed but expansion of bubbles or gravity effect is mostly dominant. Figure 2A shows a gneiss pebble where biotite strongly expanded and formed tunnels up to several cm long in the direction of stone's long axis. The melt flowing down often formed large droplets, many of which solidified prior to separation (see Figure 5). Rarely more complicated deformation is observed, pointing to softening of the rock and possibly explainable by accidental fall of the stone from the upper part of the furnace wall (Figure 6).

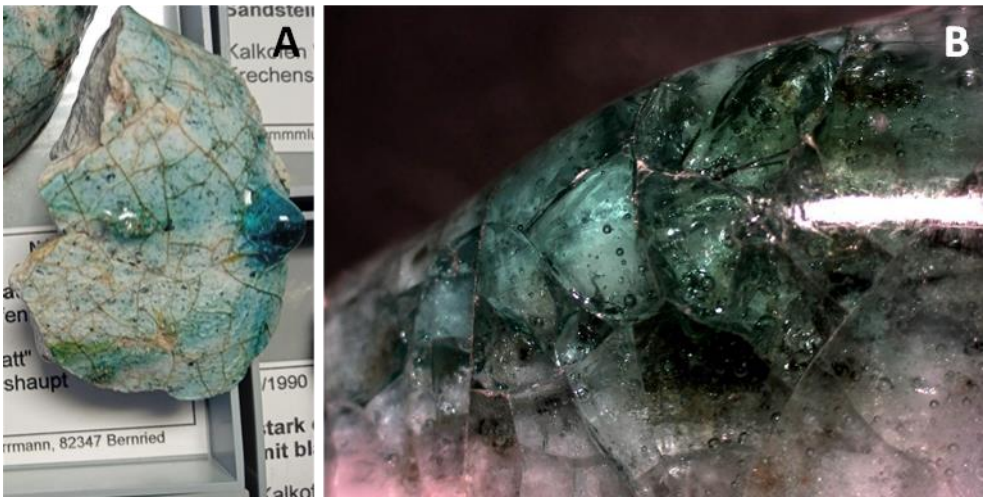

Figure 5. (**A**) Glass droplet on the former lower side of the stone (quartzite, Ko-008, Kohlstatt; image height 11 cm). (**B**) Thick green glass with signs of incipient droplet formation (gneiss, Ko-110, Tradfranz 1; image width 16 mm).

 doi:10.20944/preprints202403.1373.v1

Figure 6. An example of more complicated thermoplastic deformation observed on a gneiss sample (Ko-004, Kohlstatt; image width 13.5 cm).

Burnt loam fragments are typically flat (Figure 7), indicating intentional processing, e.g., to form covers. The morphology of burnt limestone fragments (commonly containing spheroid formations) shows that their original structure was fully destroyed (Figure 8) due to volume changes during decarbonization, followed by slow partial renewal of carbonate.

Figure 7. (**A**) Burnt loam, possibly from a cover of the kiln (Kohlstatt; image height 10 cm). (**B**) Burnt loam with imprints of twigs with needles (Rohrwies; image width 8.5 cm).

 doi:10.20944/preprints202403.1373.v1

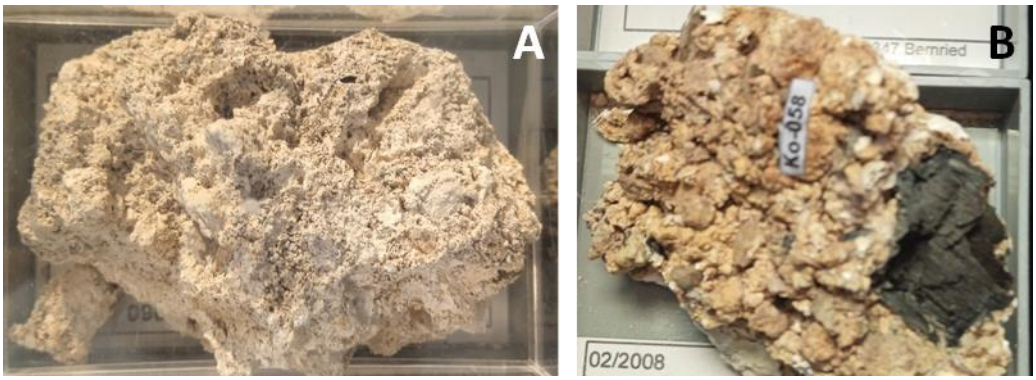

Figure 8. Partly recarbonized lime (kilns Ludwigsried I (**A**) and II (**B**), with charcoal; width of both images 8 cm).

4.2.2. X-Ray Fluorescence (XRF), Electron Microprobe (EMP)

Most surface glasses (transparent, usually of greenish or similar color) covering various types of rocks formed by silicates and quartz, have systematically high content of K and Cu and elevated Rb (Figure 9, Table A1). EMP data (Figure 10, Table A2) also confirm significant Na content, but Al concentration is usually low, precluding a dominant influence of feldspars or even micas on the glass composition. No systematic difference from the composition of typical surface glasses covering the pebbles from craters can be confirmed within the dataset available. Nevertheless, surface glasses from limekilns reach somewhat higher concentrations of Cu, Cu, and perhaps of more transition metals (Ni, Co [13]). A transitional, dark green, relatively Fe-rich glass is also common in limekilns.

Besides transparent glasses, opaque dark to black surface glasses were analyzed. They form relatively homogeneous strips and were derived from Fe-Mg silicates which had perhaps partly weathered to Fe and Mn oxides. The Ca content of surface glass is independent on the rock interior, while relatively high content of Zr and (mainly in opaque glass) Y in some analyses could be caused by accessory minerals from the rock. In addition, white K-feldspar derived glass (rich in K, Rb, and Ba) was analyzed with a semiquantitative XRF probe. For more trace elements, see also [13] for Instrumental Neutron Activation Analysis (INAA) of glass from the sample Ko-085.

In the subsurface and pebble interior mainly mafic (Fe and Ca rich) melts were analyzed (Figure 10), where newly formed crystals were found: TiO_2 phase (rutile?) and (near the surface) Fe-Al oxide (Ko-081, basic/mafic rock), probably orthopyroxene (hypersthene) (Ko-003, sandstone), and fayalite (Ko-085, amphibolite). Primary quartz has been commonly preserved. The presence of organic carbon derived particles in dark glass is possible.

The analyzed burnt calcareous loam with an imprint of spruce twig with needles contains no charcoal and is not enriched in K or other elements from biomass (with a possible exception of slightly elevated Zn and Ni).

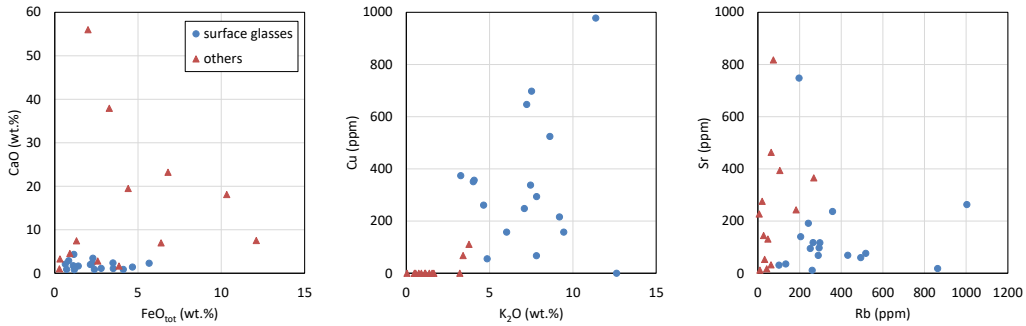

Figure 9. Binary plots of selected elements in samples from limekilns (XRF; see Table A1); "others" include rock interior and samples not affected by melting.

 doi:10.20944/preprints202403.1373.v1

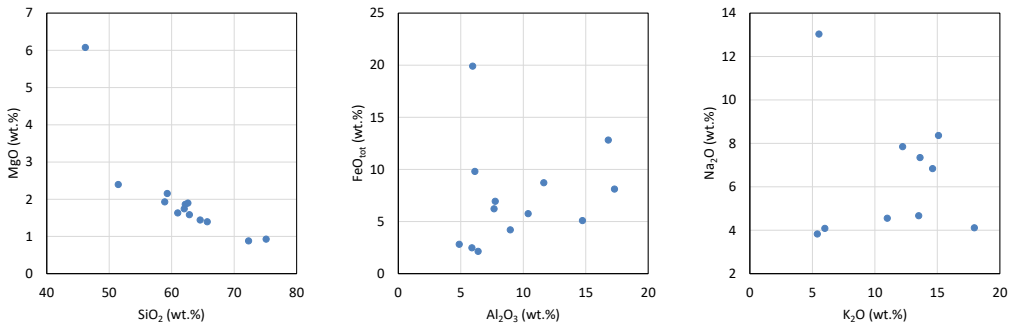

Figure 10. Binary plots of selected major components in various glasses of limekilns analyzed with EMP (see Table A2).

4.2.3. Glass Melting Temperature

Both probes of glass-dominated molten rocks (Ko-007, amphibolite, Figure 2C, and Ko-069, identified as sandstone) softened at 970 °C and melted at 1100 °C.

4.3. Petrography and In Situ Transformations – Emmerting and Kaltenbach

4.3.1. Macroscopic Deformation and High-Temperature Effects

A systematic comparison for the first 22 samples (representing 23 pebbles - two of them have been "welded" by melt) of Crater No. 4 (Emmerting; collected in 2015) is presented in Table A3. It summarizes their basic characteristics, signs of high-temperature and deformation processes, and MS values. Note that some important diagnostic minerals, including feldspars, were usually melted, so it is difficult to determine the original rock type. Ten of 23 pebbles represent silicate rocks or impure quartzite, out of which 7 are characterized by significant melting inside. The remaining 13 pebbles are sandstone, calcareous sandstone, limestone or dolomite, and vein quartz; inside of these rocks melting was not observed (not checked in two samples, probably sandstones, not broken to preserve their unique deformation features). From Crater No. 5 where younger filling prevails we investigated only three pebbles (all representing melted silicate rocks). From the Kaltenbach structure we collected mainly limestone prevailing there, and 7 silicate rock samples (see also Table A6).

Pebbles (or large fragments) with distinct open fractures found in both craters at Emmerting would hardly survive longer transport; thus the fractures must have been formed in situ. Simple fracturing was also observed in the Kaltenbach structure: an example is a limestone pebble (Figure 11) with three rheologically different inclusions (which were probably formed during the transport from Alps). The degree of filling of open fractures by secondary minerals and soil excludes that they could form during recent excavations of the site. However, explanation by common pedogenic processes is also possible.

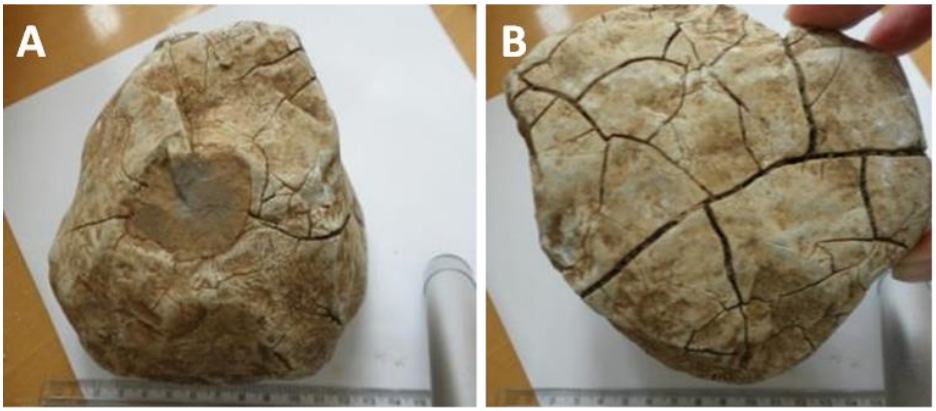

 doi:10.20944/preprints202403.1373.v1

Figure 11. Open-fracture-rich limestone pebble (Kaltenbach, #102). (**A**) Side with an older inclusion (with weathering crust) which probably influenced the fracturing, being itself only slightly fractured (image width 19 cm). (**B**) The most fractured side of the pebble; note the soil and roots in the widest fractures (image width 18 cm).

Some pebbles may have been broken-off along older fractures (Figure 12A). Many fractures are partly (Figure 12B) or nearly completely filled with melt glass. Thin transparent glass coatings may cover almost whole pebbles but not the walls of young fractures.

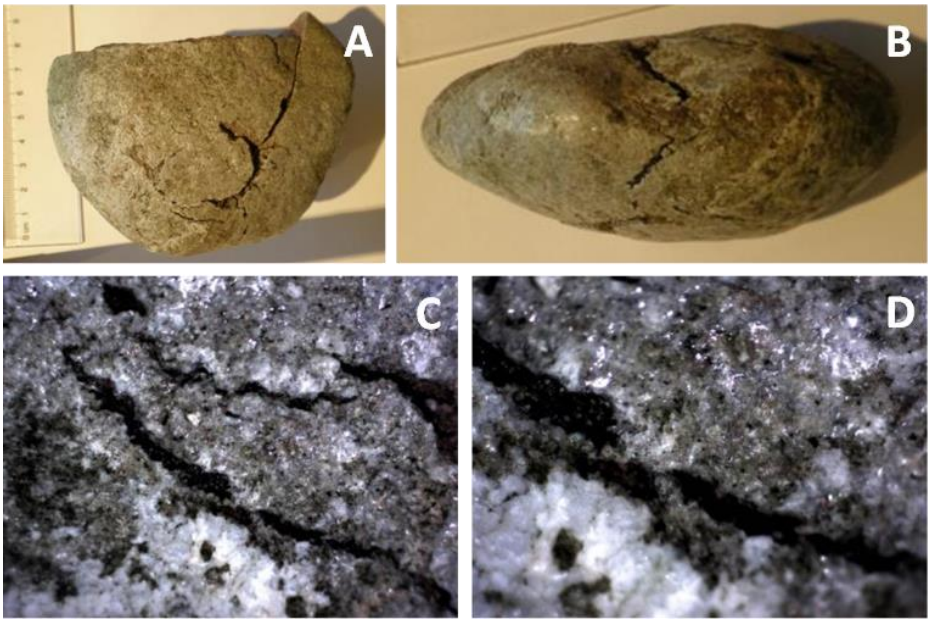

Figure 12. Fractured sandstone (Crater No. 4, #415). (**A**) A view from the probable original upper side with thin glass coating; part of the original pebble (top) was broken-off along an older crack (with limonite) after the strike (image height 10 cm). (**B**) A view from the narrow side (image width 13 cm). (**C**) Two skew bridges formed by extension of a fracture (image width 16 mm). (**D**) Detail of the same.

In the Kaltenbach structure, only three partially molten samples have been found. The surface of the sample #123 with relatively thick glass in some places shows some deformation during or after melting (Figure 13). Inside the pebble, however, significant deformation is uncertain.

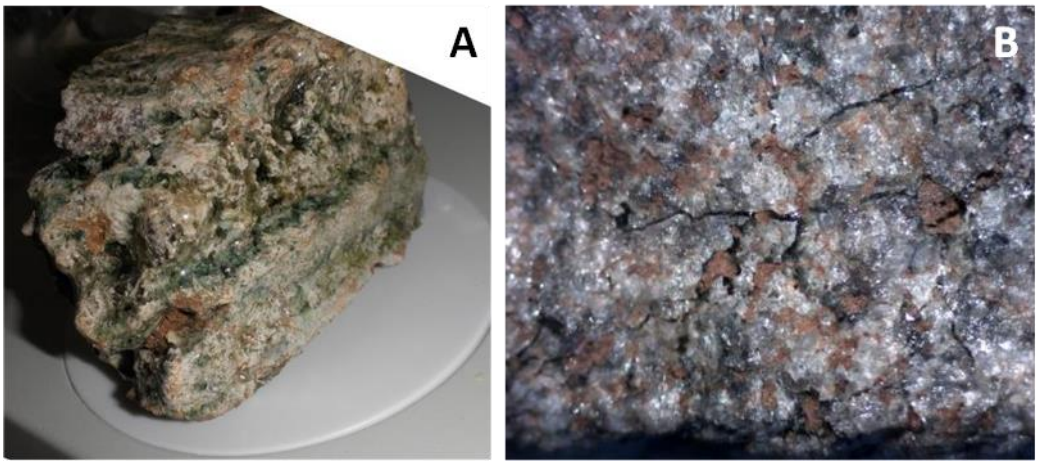

Figure 13. Partially melted orthogneiss (Kaltenbach, #123). (**A**) Ductile deformation of glass and probably of the unmolten pebble surface too. Diameter of the white circle is 10 cm. (**B**) Irregular fractures filled with glass formed from injected (?) melt; probably bottom side of the pebble (in the time of depression's formation) with no significant glass coating, dimbles are filled with soil (image width 9.3 mm).

 doi:10.20944/preprints202403.1373.v1

Open fractures are characteristic mainly for silicate pebbles from the Crater No. 4. They are often crossed by stretched bridges which evidence that extreme strain and ductile deformation accompanied the brittle deformation (Figures 12 and 14). The stretched bridges are intriguing especially in the case of individual quartz grains, possibly transformed to cristobalite (Figure 14). Their deformation is similar to lechatelierite in moldavites which may have also formed from individual quartz grains [26]. In most cases, the deformations were observed in more or less melted samples (Figures 12–17), but deformations without signs of melting inside the rock have also been observed (see 4.3.6).

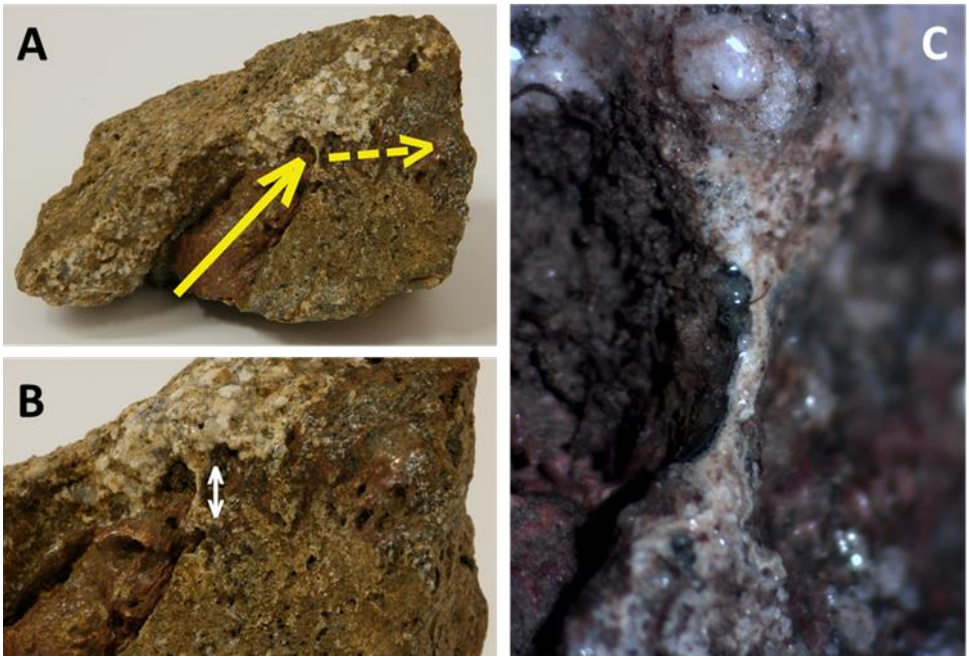

Figure 14. Extension of quartz-rich rock caused by impact of the red-colored rock fragment (Crater No. 4, #4/2/–5b). (**A**) Overview (length 10 cm). (**B**,**C**) Zoom-in views. Note that contamination with younger soil could not be fully removed.

Figure 15. A relatively large partially molten silicate pebble (Crater No. 4, #4/2/1a; image height 17.5 cm), "welded" with a basic rock on the left, and hit by secondary projectiles (calcareous sandstone).

 doi:10.20944/preprints202403.1373.v1

Note the pushing away of the partially molten surface by the projectile (small arrows), and the furrows behind the projectile (larger arrow).

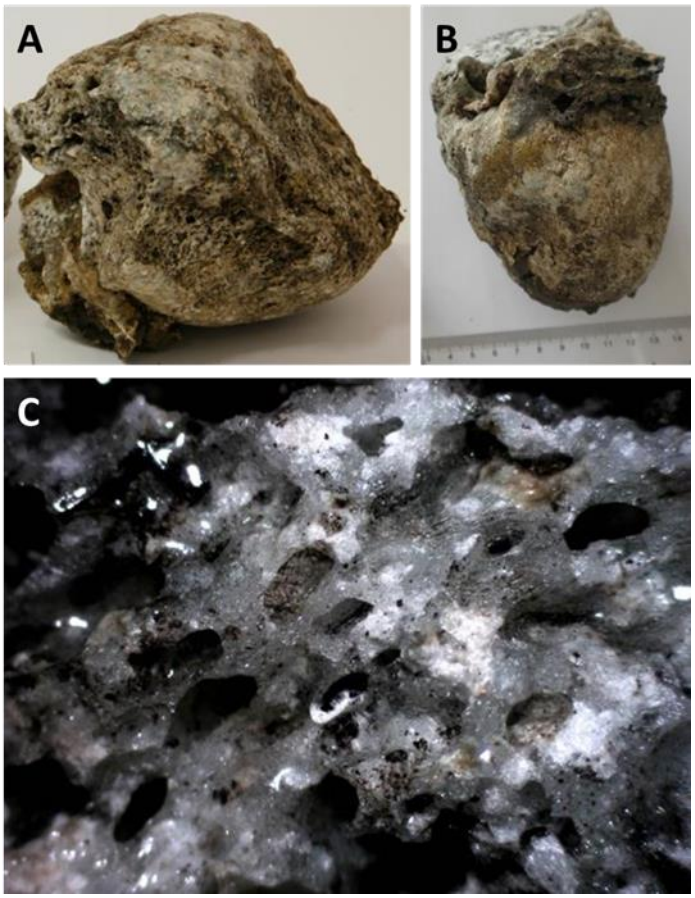

Figure 16. A strongly expanded pebble (Crater No. 4, #4/2/–1b). (**A**,**B**) Overview (image widths 14 and 12 cm, respectively); see also the dark, strongly deformed melt – possibly a secondary projectile (image (**A**) – in the left bottom, image (**B**) – in the top). (**C**) Original surface (relatively thin cutting on black background). Image size 12×16 mm.

 doi:10.20944/preprints202403.1373.v1

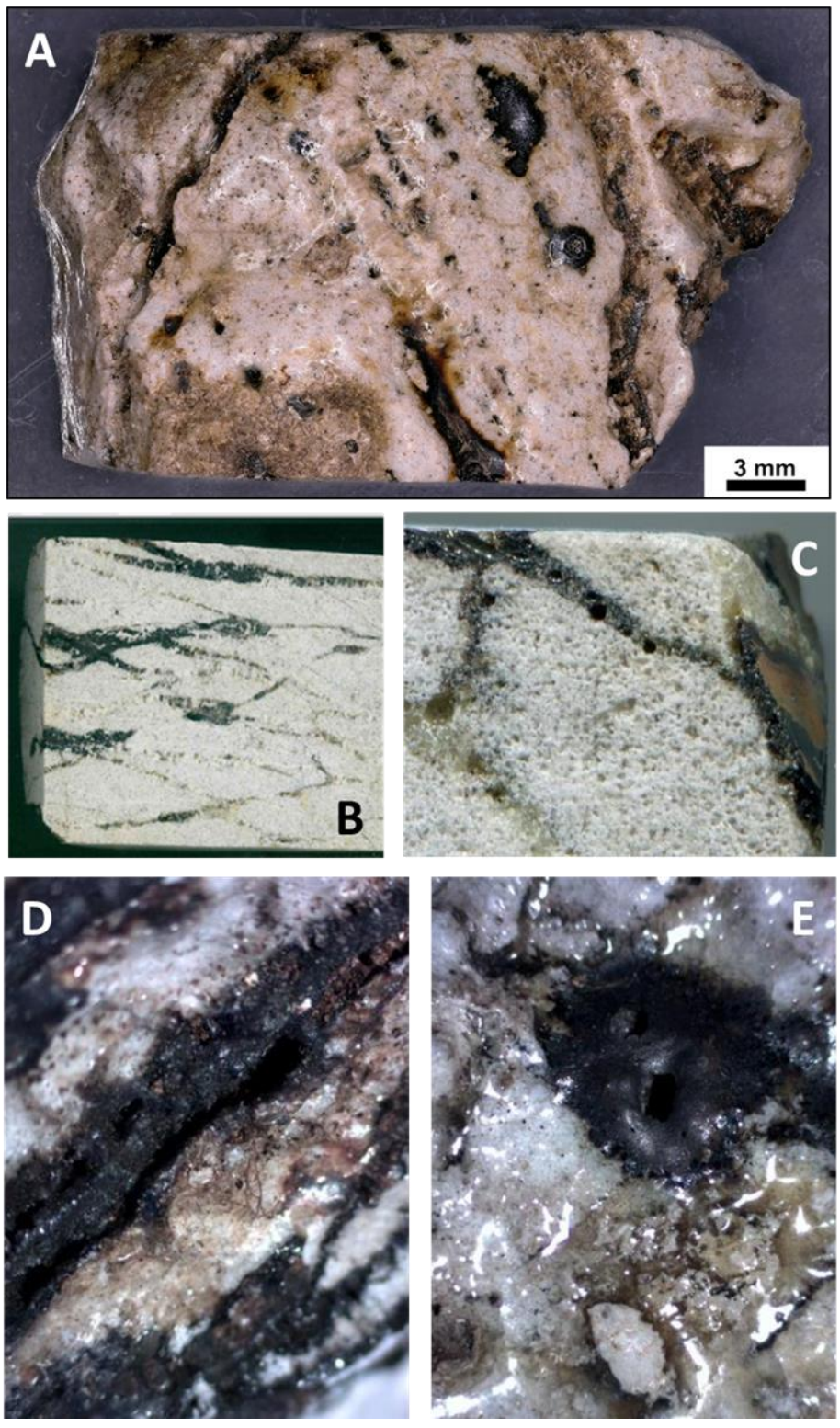

Figure 17. Impure quartzite (Crater No. 4, #421). (**A**) Parallel extrusions of dark melt. (**B**) Dark melt veinlets and white tectonic quartz veinlets in unpolished section. Image height 3.5 cm. (**C**) Extrusion of melt from interior on the pebble's surface, also forming a thin surface reaction layer (brown). Image height 9 mm. (**D**) Open fracture partly filled with dark melt. The light bands are formed mainly by quartz with minor portion of glass (surface of a fresh fracture after breaking of the sample). Image size 16×12 mm. (**E**) Extrusion of dark melt on the surface formed by colorless and yellow glass with abundant bubbles. Image size 16×12 mm.

 doi:10.20944/preprints202403.1373.v1

Micas, feldspars, or both either melted in the whole pebble, or not at all. Eutectic melting inside the pebbles, if visible, is very limited. Significant expansion was documented in several samples where typically micas (especially altered biotite) dehydrated, melted and solidified to glass, with abundant microscopic skeletal magnetite and locally other minerals formed from melt. In places, the gas may have liberated with some delay after melting (unmixed during cooling?).

Evaporation of silicates in the Crater No. 4 is evidenced. The sample #4/2/–1b (originally perhaps granitic or dioritic rock) is very strongly expanded, weighing less than 600 g despite its dimensions (ca. 8–13 cm; Figure 16). It also displays significant strain and deformation, possibly due to impact of a secondary projectile.

Secondary projectiles are observed which strongly deformed the partially molten surface (Figure 15), or penetrated deep into the pebble probably using the space made by older discontinuities (Figure 14). These impacts also lead to injections of melt (see 4.3.6). The most typical secondary projectiles formed by melting of mafic rocks like amphibolite.

In both Crater No. 4 and Crater No. 5, the mica-derived melt formed conspicuous extrusions on the surface, mainly on impure quartzite pebbles (Figures 17 and 18). Dark porous melt which resembles miniature "cinder cones" (see Figure 18B) or is flat and seemingly similar to lichen, was expelled from veinlets. These extrusions could have been propelled by gas unmixed during melt cooling. The transparent glass coatings never cover the porous dark melt, which holds for extrusions as well as secondary projectiles. It follows that the mafic melts were still very hot (or even not yet covered the surface of pebbles) when the thin, usually colorless glass coatings were already solidifying. This is also supported with chemistry of the glass coatings which is almost unrelated to that of the pebble's rock (see 4.3.5).

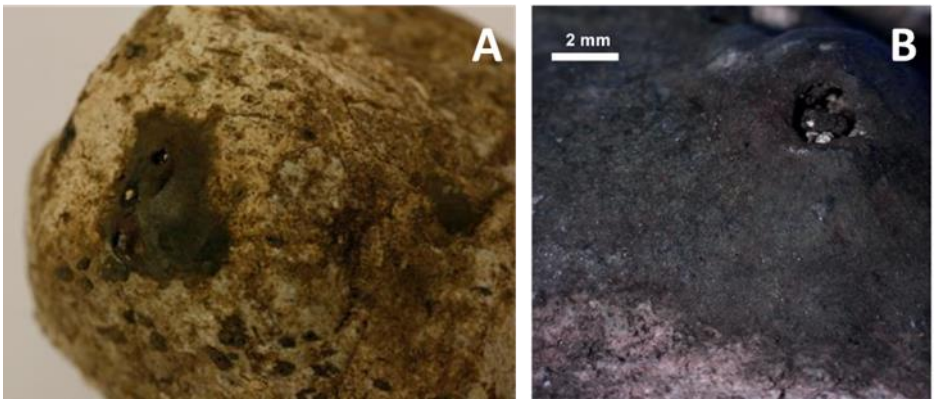

Figure 18. Extrusions of dark melt in micaceous quartzite (Crater No. 5, #5/1/0a; image width 9 cm). (**A**) The largest extrusion on the pebble's surface (smaller extrusions are rather flat, resembling lichen. (**B**) Zoom-in view.

The quartzite sample #421 is a typical example of longer duration of the high temperature (probably due to a high amount of melt at the crater bottom), enabling crystallization of various minerals (see 4.3.4 and Table A4), which does not contradict quick and disequilibrium melting. Also pebbles welded by melt, without significant mutual deformation, were found at the crater bottom (#407 – see Table A3).

4.3.2. Decarbonization

Probable remnants of re-carbonized lime are found in all three crater-like structures. Importantly, in some samples evidence of in situ decarbonization can be observed. Part of the surface of the sample #5/1/0a, especially near the crossing of two fractures (former calcite veinlets?), is covered with a white "mortar", containing stuck grains of, e.g., quartz from the surrounding soil/sediment (Figure 19). The mortar formed naturally from re-carbonizing lime, and it is younger than the glass coating.

 doi:10.20944/preprints202403.1373.v1

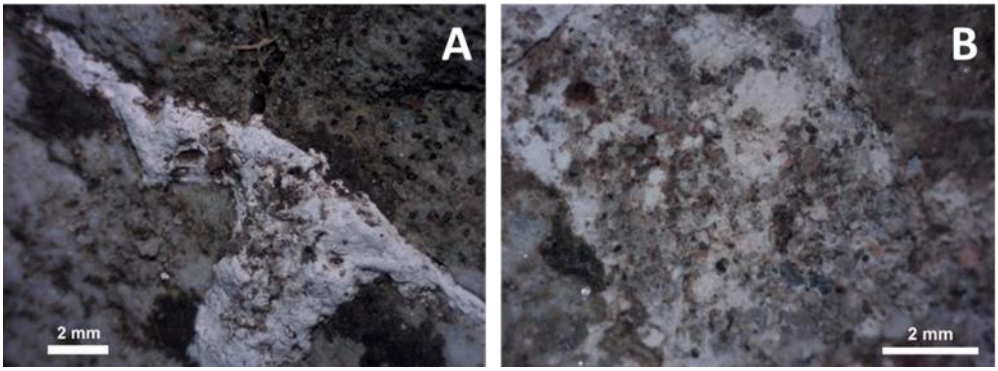

Figure 19. (**A**) White "mortar", i.e., small mineral (e.g., quartz) and perhaps organic grains stuck on the original lime on two intersecting cracks (Crater No. 5, #5/1/0a). (**B**) A detail of mortar with stuck grains, on the bottom left and upper right also (older) thin glass coating is visible.

It has never been observed in the present study that glass would cover carbonates. It seems that the pressure of escaping gas (CO_2) prevented formation of any continuous coating at high temperature; nevertheless, glass sometimes formed on older weathering crusts of carbonate pebbles. Possible product of reaction of an external hot material with carbonate is the matter similar to pumice observed in Crater No. 4 (#417 - sandy limestone; Figure 20A) and perhaps in Crater No. 5, partly filling open fractures and/or covering pebble's surface. Its bright colors and relatively hard and inflexible consistency exclude organic character (also XRF, where applicable, shows a silicate composition). This "pumice" could be a product of a reaction of glowing fluid, melt or aerosol from outside with the original surface, strongly influenced by escaping gas (especially on calcite veinlets or carbonate surfaces). Charred, obviously burnt relics of moss were also found on relatively sheltered surface of the sample #417 (Figure 20B).

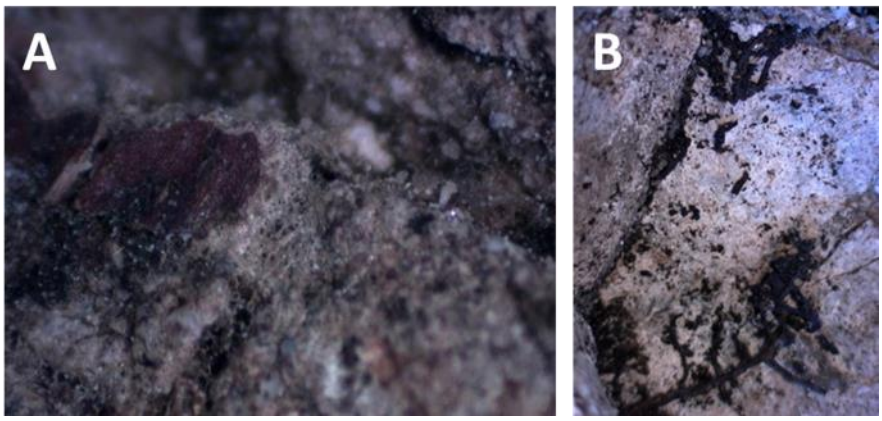

Figure 20. (**A**) A leaf remnant (rusty) stuck on yellow porous glass(?) layer ("pumice") on an impure carbonate pebble (Crater No. 4, #417). Image width 3.1 mm. (**B**) Charred moss at another site of the same sample. Image size 12×16 mm.

Unusually complicated morphology, rough surface and easy disintegration are also typical for many small (several-cm sized) carbonate fragments, especially in Crater No. 4, and similar crust also covers a dolomite pebble (Figure 21A). We suggest that the decarbonization phenomena took place, which could also explain the bright white, soft, chalk-like surface of many pebbles of Crater No. 4 and the Kaltenbach structure. Nevertheless, many limestone samples (including large ones) do not display such an effect.

 doi:10.20944/preprints202403.1373.v1

Figure 21. (**A**) "Flourishing" of dolomite surface, perhaps due to gas expansion during decarbonization (Crater No. 4, #406). (**B**) Partly decarbonized limestone (Kaltenbach, #105): outer carbonate zone and inner zone with relics of lime (portlandite). Image width 9 cm. (**C**) Probable relics of mortar on the surface of the same sample.

In the sample #105 from the Kaltenbach structure, residual lime (portlandite) was identified. Its partial re-carbonization formed a macroscopically distinct crust; in addition, matter similar to man-made mortar occurs on the sample surface (Figure 21B,C).

Similar to limekilns, gas liberated from carbonate may also have helped to expansion of Ca-rich silicate rocks (#419, Crater No. 4; see also 5.5).

4.3.3. Mineralogy: Primary Minerals and Their Transformations

Mineral composition of representative silicate samples is shown in Table A4. Inside some samples, the mineral composition has not significantly changed during the crater-forming process. This holds mainly for carbonate pebbles and for sandstones from the Kaltenbach structure.

The remarkably deformed (possibly partly mylonitic) sample #422 (Crater No. 4), containing chiefly quartz and albite, also shows no melting (the thin surface glass has an external source – see below); the only possible thermally induced mineral transformations are decomposition of chlorite (which is relatively opaque) and dehydration of limonite, which perhaps formed opaque rims at some grain boundaries. Strong fracturing of both quartz and albite is observed, including some planar fractures in quartz and highly intense cleavage of albite (Figure 22); however, these features have not proved shock metamorphism yet.

Complete melting of feldspars and micas is common in Crater No. 4, which is indirectly documented with absence of their crystals in the most of samples and directly by composition of glasses. An extreme case is the sample #16133 where glass pseudomorphs after K-feldspar (with abundant bubbles; see also 4.3.4) seem to have completely unchanged chemical composition of the original feldspar, and the same probably holds for original albite exsolutions in the same sample (see Table 2).

 doi:10.20944/preprints202403.1373.v1

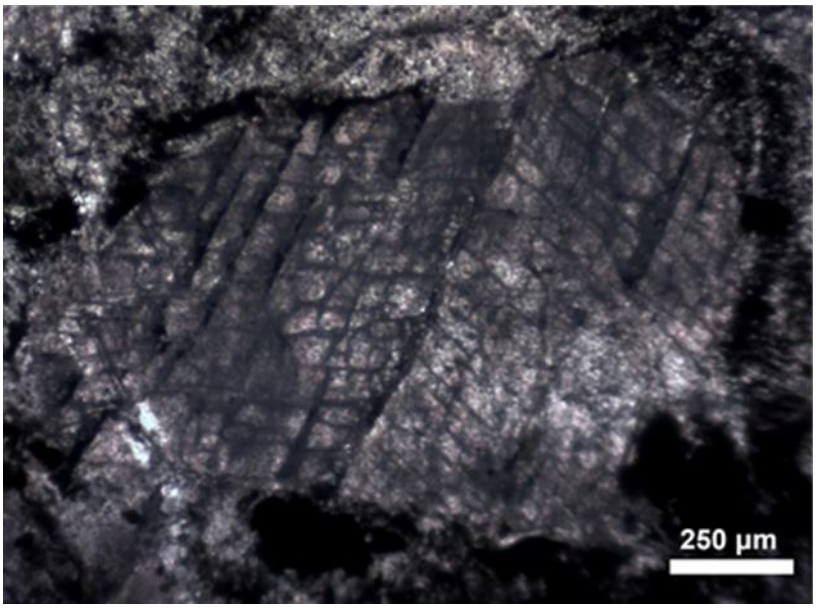

Figure 22. Intensely cleaved albite (Crater No. 4, #422; transmitted light).

Table 2. EMP analyses of glass in selected samples (oxides normalized to the sum of 99 wt.%; arithmetic mean).

Sample No.	glass type	*n*	SiO_2	TiO_2	Al_2O_3	FeO_{tot}	MgO	MnO	CaO	Na_2O	K_2O
123	feldspar-equivalent	10	65.08		19.00	1.10				5.32	8.45
123	Fe-enriched	6	65.72		15.41	6.05	0.08		0.08	4.70	6.70
420	most analyses near surface	12	65.13	≤ 0.20	14.62	3.34*	0.99	≤ 0.20	3.25	5.86	5.62
421	dark glass	4	66.82	0.36	10.12	16.86	0.25	1.28	0.17	2.97	0.06
421	relatively bright, interior	5	70.72	0.67	14.95	5.64	0.61	0.48	0.44	4.57	0.63
421	relatively bright, near rim	11	68.76	0.60	10.31	5.09	1.25	0.58	4.45	4.46	2.23
15240	inner surface	1	81.51	0	4.21	1.14	2.56	0	2.05	3.46	4.23
15240	outer surface	1	80.11	0	5.67	1.12	1.01	0	2.51	3.78	4.91
16133	Kfs-pseudomorphs	11	65.34		18.18	< 0.20				0.61	14.84
16133	injections	6	61.34	≤ 0.20	14.86	3.87	1.05		4.63	0.70	12.31

* $Fe_2O_{3\ tot.}$

Primary cristobalite (scale-like; see also [25]) was not observed in any sample. Zircon and less frequently monazite, rutile and rarely xenotime are primary accessory minerals preserved in glasses in various samples. They are often intensely fractured and even penetrated by the glass (see 4.3.6). In contrast, in intensely melted but not significantly deformed quartzite sample #421, the disturbance of zircon is minimal. Baddeleyite (ZrO_2) as a high-temperature product of zircon decomposition was not observed. The temperature of zircon-to-baddeleyite transition in long-lasting industrial processes is considered to be about 1550 °C [25]; however, for shock metamorphism, temperatures up to 1800 °C are reported [27].

Fluorapatite was only observed in the sample #421. It is highly porous and corroded, which can be explained by dissolution in the melt (or volatilization), but also by previous weathering or hydrothermal alteration. Crystallization of F-free Ca phosphate and P-rich pyroxene from the melt at the Ca-enriched rim of the same sample could imply some dissolution of apatite; alternatively, P may have originated from organic contamination.

 doi:10.20944/preprints202403.1373.v1

4.3.4. Glasses and Secondary Minerals: Microscopy, Microchemistry

In several feldspar-poor samples, only dark glass is found. In the quartzite #418, the dark biotite-derived glass merges into brightly red Fe-oxides which are porous in places but probably anhydrous, as evidenced by very high MS of the pebble. It can be inferred that the original biotite (chlorite?) had been limonitized prior to crater formation, especially near the pebble's surface. During crater formation, limonite and biotite/chlorite were dehydrated. Also note that this sample (Figure 23) has no surface glass of "external" origin, showing that melting inside pebbles and formation of surface glasses were largely independent processes.

Another example of disequilibrium melting of micas and their alteration products, accompanied by expansion, is the blue-green glass in the sample #407 (Crater No. 4), chemically little different from biotite. Similarly, in orthogneiss from the Kaltenbach structure (#123) where biotite had probably been previously altered to chlorite and other secondary minerals, relatively dark green, Fe-enriched, strongly expanded melt formed from "biotite" (Figure 24). The coexistence of feldspar glass with small pores/bubbles, colored and expanded mica-derived glass, and unmelted or only slightly melted quartz is typical. Crystalline character of quartz is confirmed by birefringence (in thin sections) or by diffraction peaks in XRF spectra. In some cases, the feldspathic melt starts to mix with biotitic melt (sample #16131) and may be locally influenced by limited dissolution of quartz. Secondary cristobalite was found in the sample #421 (Crater No. 4) and very rarely in #123 (Kaltenbach), forming microscopic crystals to dendrites on the surface of quartz grains in glass (i.e., crystallized from SiO_2-rich melt). Impurities such as Al, Na, and Fe are common in cristobalite.

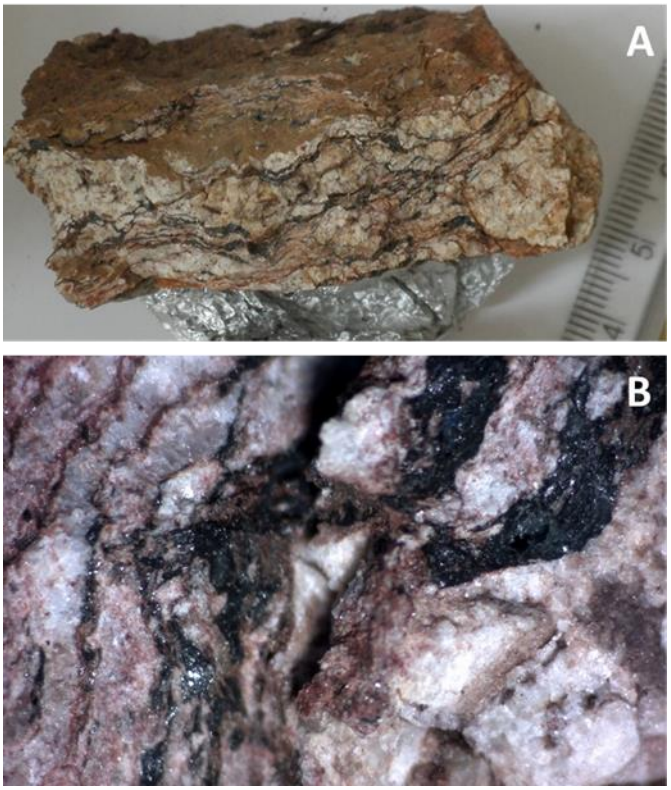

Figure 23. (**A**) Dark, little expanded glass likely derived from biotite, with continual transitions to limonite or hematite, in quartzite without quartz melting (Crater No. 4, #418). (**B**) Zoom-in view. Image width 7.9 mm.

 doi:10.20944/preprints202403.1373.v1

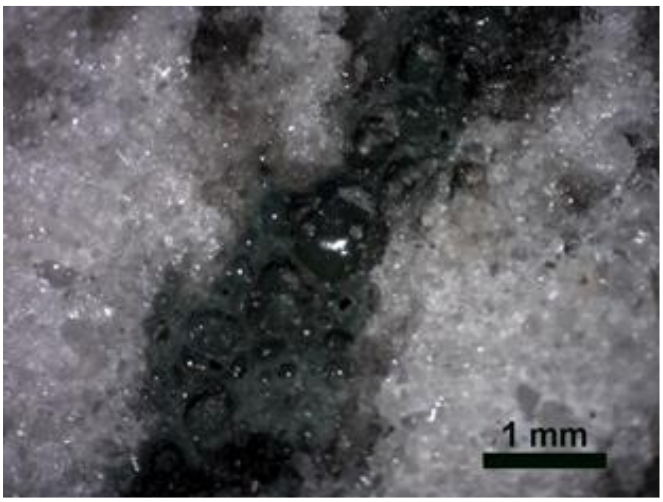

Figure 24. Porous green melt formed from previously altered biotite in orthogneiss (Kaltenbach, #123).

Melting of albite and partly quartz may explain glass composition in the sample #16129 which, however, is porous and expanded, and so intense evaporation may have taken place. In the sample #16133, the original K-feldspar had been penetrated by quartz veinlets which have been preserved without any reaction with the feldspar glass (Figure 25). The glass penetrating into the sample from the surface is also relatively K-rich and Na-poor, but with significant admixtures of Ca, Fe and Mg (Table 2).

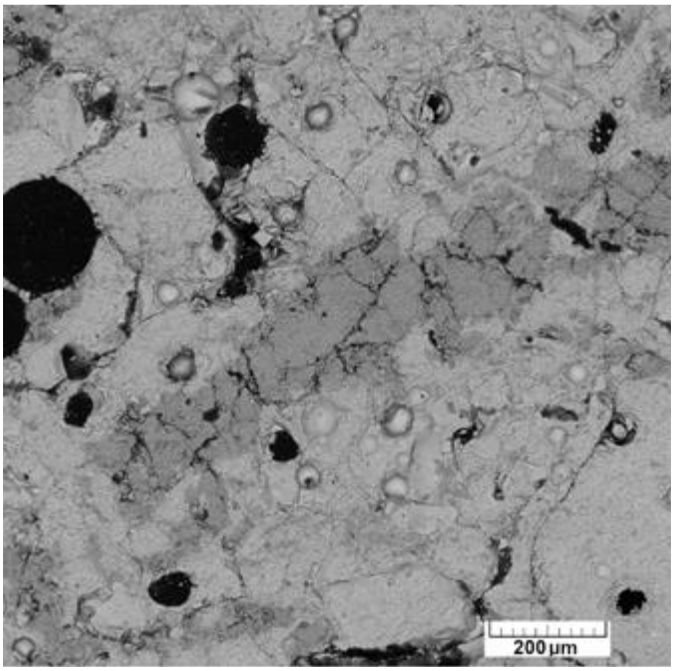

Figure 25. Quartz veinlet (medium grey) in a glass pseudomorph after K-feldspar (light grey, rich in bubbles) (Crater No. 4, #16133).

Twelve EMP analyses of thin (<1 mm) colorless subsurface to surface glass originate from a granitic pebble (Crater No. 4, #420). In few cases, the composition is similar to ternary Na-K-Ca feldspar (4 analyses) or to feldspar with Al partly substituted by Fe (3 analyses). The remaining analyses show excess of alkalis not only in relation to Si but also to Al, and/or excess of Fe. In this small dataset, K is negatively correlated with Na and Al but not with Ca, Mg or Fe (Figure 26). It can be inferred that mainly feldspars were the "internal" source of melt, but K is also significantly

 doi:10.20944/preprints202403.1373.v1

enriched in outermost glass, probably due to contamination with plant-derived material. In the glass also acicular diopside and plagioclase were found, formed by rapid crystallization from melt or crystallization from the glass (see Figure 27). The diopside ($Na_{0.056}K_{0.045}Ca_{0.91}Mg_{0.58}Fe_{0.3}Mn_{0.063}Al_{0.1}Si_{1.97}O_6$, approximate formula) morphologically resembles its form which can occur as a defect in cooling industrial glasses at temperatures of ca. 1100 °C [25]. Iron-rich (hedenbergite-like) clinopyroxene was found in the near-surface glass (enriched in Ca due to contamination; see Figure 28) of the sample #421; this pyroxene also contains significant admixture of P.

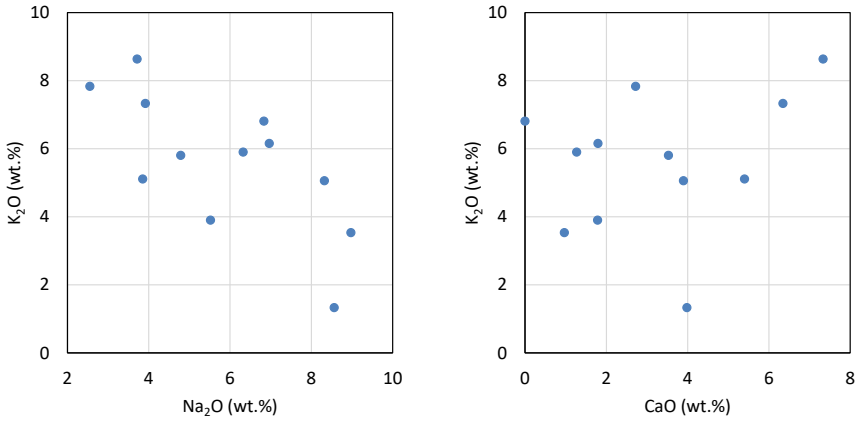

Figure 26. Plots of K_2O vs. Na_2O and CaO with (oxide wt.% normalized to a total of 99 wt.%) in surface or near-surface glass of sample #420 (Crater No. 4).

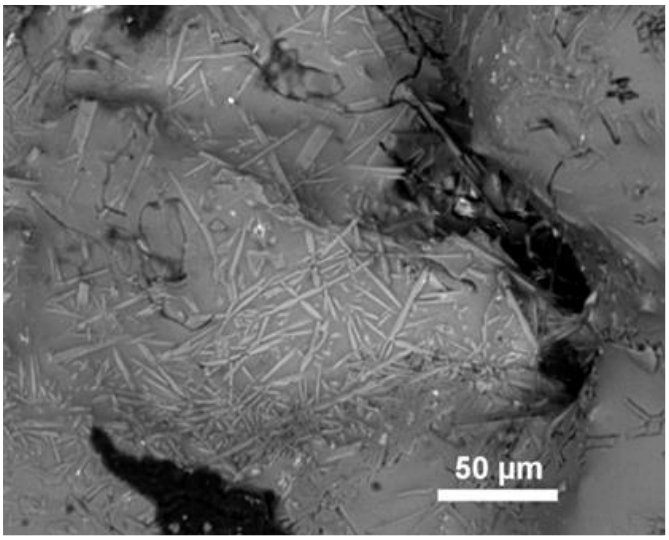

Figure 27. Acicular crystals, among which diopside and plagioclase were identified (Crater No. 4, #420; BSE image).

Quite common are skeletal crystals (or dendrites) in glass, the most typical being magnetite in brown glass in the sample #421 (Figures 28 and 29), where also dendrites of hedenbergite and spherolites of Fe-rich silicate (olivine?) were found. Analyses of magnetite in samples #421 and #16131 show that Al, minor Mg and locally Mn or Ti are the only relevant isomorphic admixtures. In the sample #420 we also observed Mg-Fe rich oxide (perhaps magnesioferrite), forming clusters of small, quite isometric crystals, and unidentified (due to very fine aggregates) Mg-Al rich minerals. In contrast, Cr and Ni contents (as potential indicators of meteoritic contamination) are usually too low to be quantified by EDS in both Fe-rich minerals and glasses. Secondary Ti-oxide minerals are common in most of the mica-derived melts. Optically, probable magnetite dendrites in brown glass were also observed in the sample #16133.

 doi:10.20944/preprints202403.1373.v1

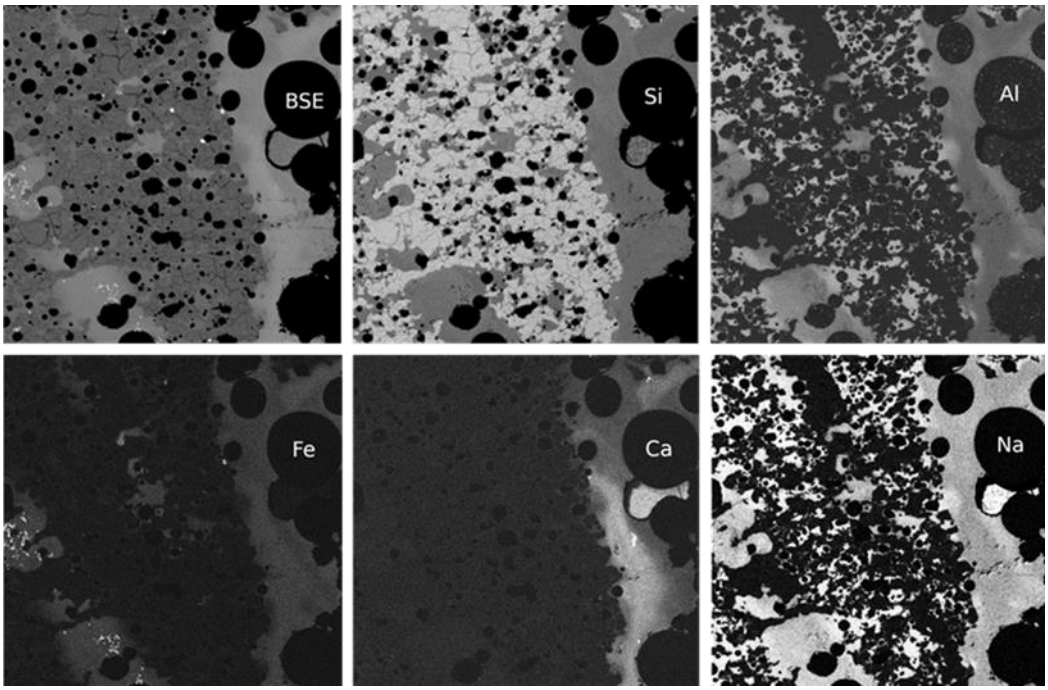

Figure 28. BSE image and concentration maps of 5 elements near the rim of a quartzite sample (Crater No. 4, #421): surface glass (colorless to light brown in transmitted light) with large pores on the right; the interior is formed mainly by quartz, glass with composition similar to albite (colorless in transmitted light), and more porous, optically dark glass with magnetite. Image size 2.5×2.5 mm.

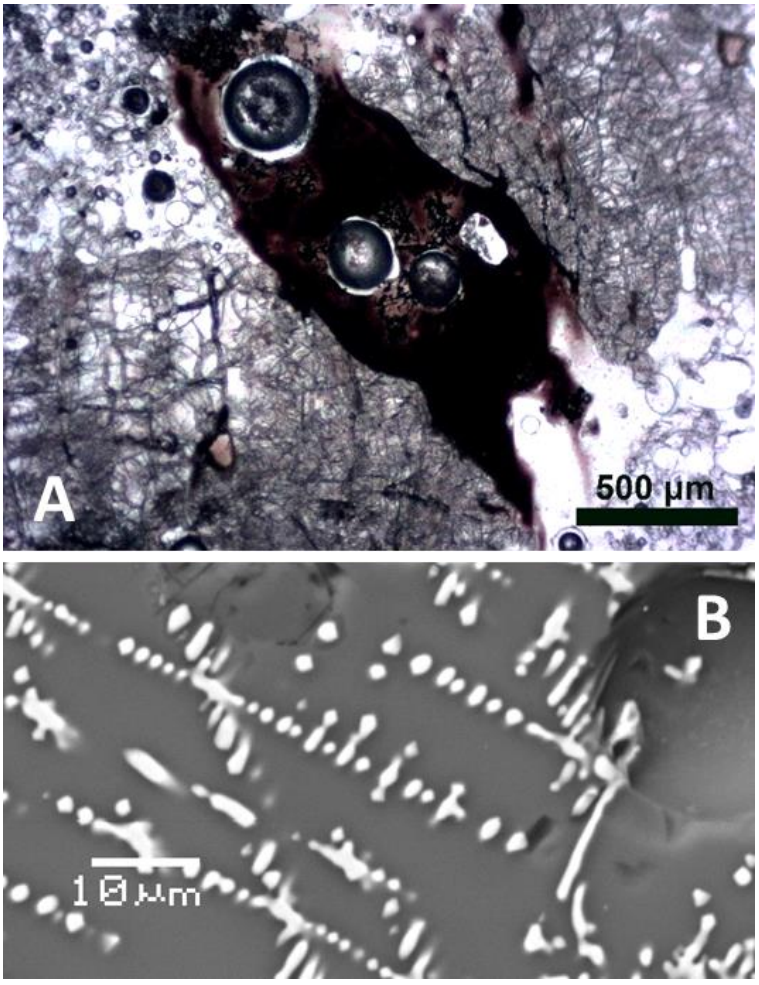

 doi:10.20944/preprints202403.1373.v1

Figure 29. (**A**) A macroscopically black, porous veinlet intersecting an older quartz veinlet. Note the heavy post-tectonic fracturing of quartz. Black magnetite dendrites in the dark vein are surrounded with translucent, Fe-depleted glass (Crater No. 4, #421). (**B**) A detail of magnetite dendrites in the same sample (BSE).

Highly interesting is mineralogy of the dark melt which was injected (by impact and melting of a secondary projectile) into the sample #16132; see 4.3.6. Crystallization in cavities is important in the biotite-derived glasses, like in the sample #16131. Mainly tabular crystals of Fe-oxides form on the inner surface of cavities. In contrast, skeletal magnetite (e.g., in the sample #421) is most concentrated in the glass near the outer side of cavities.

4.3.5. Bulk Composition of Surface Glasses and Comparison to Pebble Interior

The sample #15240 (quartzite with biotite, Crater No. 4) is an example of pebble with some fracturing, insignificant deformation, no melting inside, but with a thin glass coating (transparent, green-yellow). Neither significant reaction of the melt (glass) with mineral grains, nor thermally induced fracturing of quartz was observed (Figure 30A). Two glass layers were identified (Figure 30B) but with a similar chemical composition (Table 2). The glass sometimes covers old weathered or even moss/lichen-covered surface. It follows that the glass-forming "external" material reacted with the pebble surfaces minimally. Note that in places thin glass also covers vein quartz (which again supports external origin of the glass, unless temperature 1700 °C was exceeded).

In-situ analyses of various crusts and coatings, especially of the melt-derived ones, were performed mainly by XRF (Table A5). Weathering crusts were documented on calcite-rich pebbles (samples #409 and #417), showing relative enrichment in Sr (concentrated more than Ca in non-carbonate minerals) in surface or subsurface layers.

The thin surface glass coatings (usually colorless but also greenish or bluish) are generally remarkably rich in K, usually also Cu, partly Rb and Zn (see also [23,28]). Concentration of K also holds for glass covering weathering crusts of limestone pebbles. The glasses on Ca-poor silicate rocks are relatively enriched in Ca compared to the pebble interior. In the Kaltenbach structure, the surface glasses are not so enriched in K and Cu, and the relatively thick green glass on the sample #123 seems to be derived from the rock interior (from which it is not clearly separated), with local surface contaminations (documented by slightly elevated Cl and S, similarly to S and P in surface glass of the sample #422 from Crater No. 4).

The results do not support significant meteoritic contamination. The peak content of Ni (82 ppm) of several analyses of the brown melt quartzite samples, with high Fe/Ni ratios (> 650, if Ni was detected), corresponds to basic(-intermediate) rock material, or can be possibly explained by melted limonite from the original surface.

Several elements which were relatively reliably quantified by various XRF devices used are presented in Figure 31 and Table A5 (for light elements like Al and Si, XRF in the air is insufficiently sensitive and quantification is less precise). Out of other elements, we can mention relatively high Nb and Sn, and low Zr in the sample #123 (confirming the highly differentiated - acidic character of the original granite), elevated Zr in quartzite (#421), and significant admixture of Pb in coatings on some vein-quartz samples (most likely from oxidized sulfides). In accordance with gamma-ray spectrometry, all analyses showed low or average U content (0-4 ppm), testifying for chemical weathering (note relatively high detection limits for Th). See also the companion paper [13] for INAA analyses of glasses from the pebbles #4/2/1a (Crater No. 4) and #123 (Kaltenbach).

 doi:10.20944/preprints202403.1373.v1

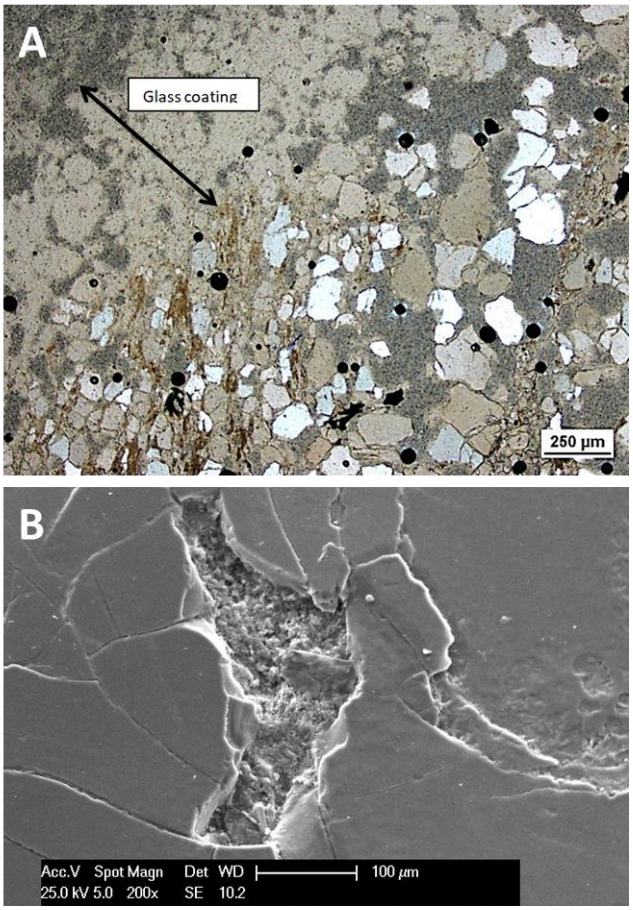

Figure 30. A quartzite pebble (Crater No. 4, #15240) containing altered biotite and organic matter, with glass coating (independent on the foliation). (**A**) Transmitted light, askew-crossed polars (hollows in the section are greenish gray). (**B**) SEM image of the surface: a flat upper glass layer (left, lower right), lower glass layer (upper right), and rugged older weathered surface of the pebble (middle).

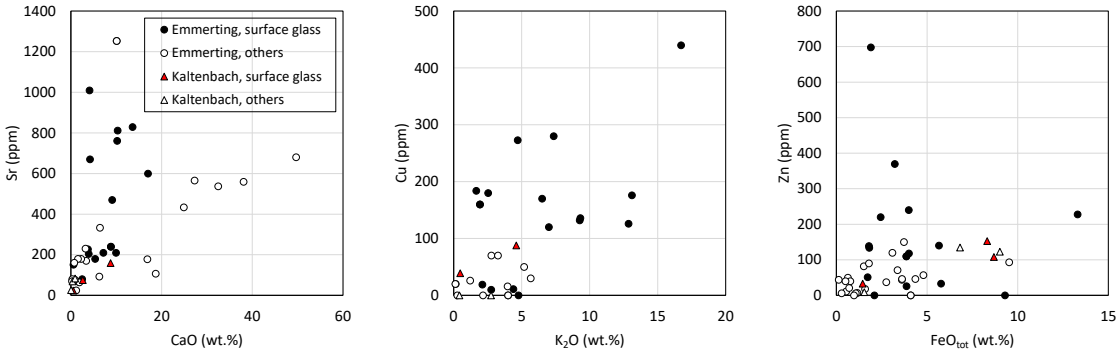

Figure 31. Binary elemental plots for samples from Emmerting and Kaltenbach (determined by XRF; see Table A5 for data); "others" include rock interior and occasionally weathered surfaces (not affected by melting).

4.3.6. Closer View of Deformation and Melt Movement in Pebbles

The highly fractured and deformed sample #422 (see Figure 32) was also investigated with CT. Results indicate little distinctive orientation of mineral grains askew to the pebble's long axis. The open fissures formed perpendicularly to the propagation of pressure (shock) wave after the compression ceased and correspond to failure by tensile stress. Fissures at the end which was

 doi:10.20944/preprints202403.1373.v1

somewhat broken off reach to the surface and are more opened than those at the opposite end. The fractures in two dominant directions may have formed by combination of the incident pressure (shock) wave and waves reflected from the opposite surface (Figure 32D). The morphology and spatial arrangement of fractures resemble, for example, rocks after tensile test with an explosive.

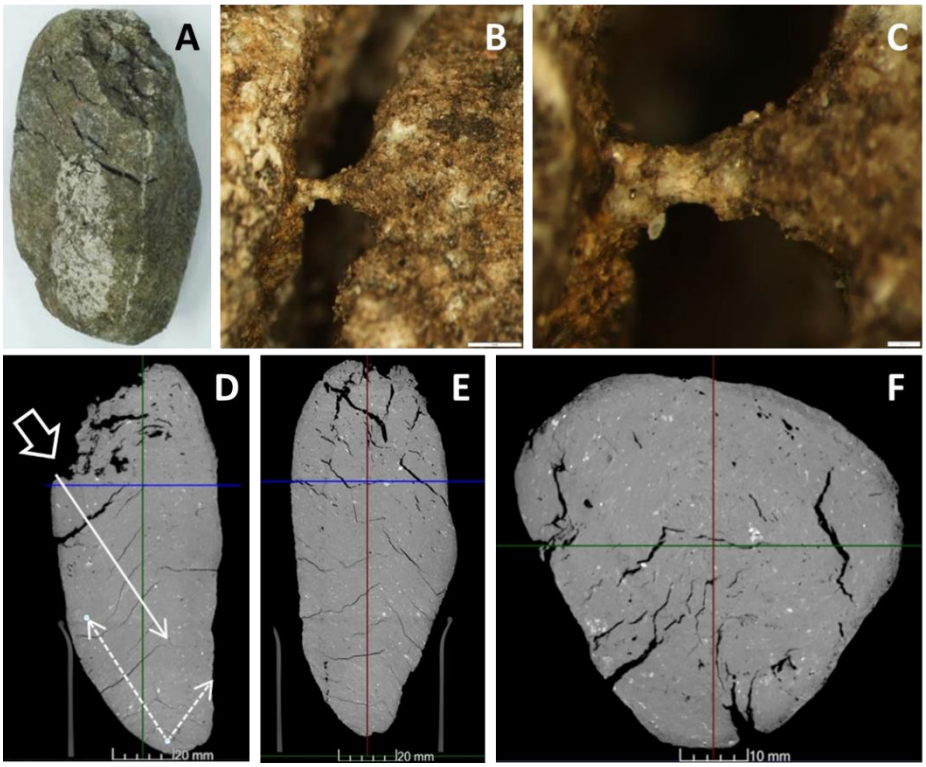

Figure 32. Fractured pebble (Crater No. 4, #422) of quartzitic or granitic rock with stretched bridges in open fractures. (**A**) Overview; note that no movement along fractures can be observed. Image height 12 cm. (**B**,**C**) Details of a bridge crossing an open fracture; it is formed by unmolten quartz and other minerals similar to the surrounding rock (scale bars 1 and 0.2 mm, respectively). (**D**–**F**) CT of the pebble in three perpendicular sections. Regular fractures are distinctive especially in the longitudinal sections. The upper arrow marks the direction of incident pressure, the bottom dashed ones mark the pressure (shock) waves reflected from the pebble's surface.

Injections of melt from outside into the pebbles were also observed, the most prominent ones in the sample #16132. The original quartzite was contaminated by dark basic melt which not only forms part of the surface but also intruded into open pores and fractures (Figure 33). These fractures partly formed and/or widened under high strain, as evidenced by stretched bridges. As a result, there are abundant planar cavities in two directions (Figure 33A), one probably corresponding to foliation; they intersect older tectonic quartz veinlets. The pebble is in places coated by thin transparent glass which, however, never covers the dark melt. Note that basic rocks may have been melted more easily than quartz due to insufficient time for eutectic reactions of quartz (in addition, the basic rocks are usually more or less weathered and hydrated).

The melt including glass matrix is basic and rich in Fe, Mg, Ca and Ti, which is very contrasting to the host rock; low contents of Ni and Cr exclude meteoritic material. Newly formed minerals include plagioclase, clinopyroxene, and olivine (or orthopyroxene). The crystals (including skeletal crystals or dendrites) in glass matrix are very tiny and quantitative microanalysis is usually impossible. Crystals also grew in spherical cavities. These are mainly Fe oxides (magnetite?) and columnar, lath-shaped to acicular pyroxene and plagioclase (Figure 33E). The only primary mineral observed of the basic rock is a Fe-Ti-Mg oxide (perhaps Mg-rich titanomagnetite). It is heavily disintegrated (crushed?) and has complicated spatial relations to the melt (Figure 33F). Fractured quartz and zircon grains of the original quartzite are almost completely surrounded by the basic melt, but without any reactions with that melt.

 doi:10.20944/preprints202403.1373.v1

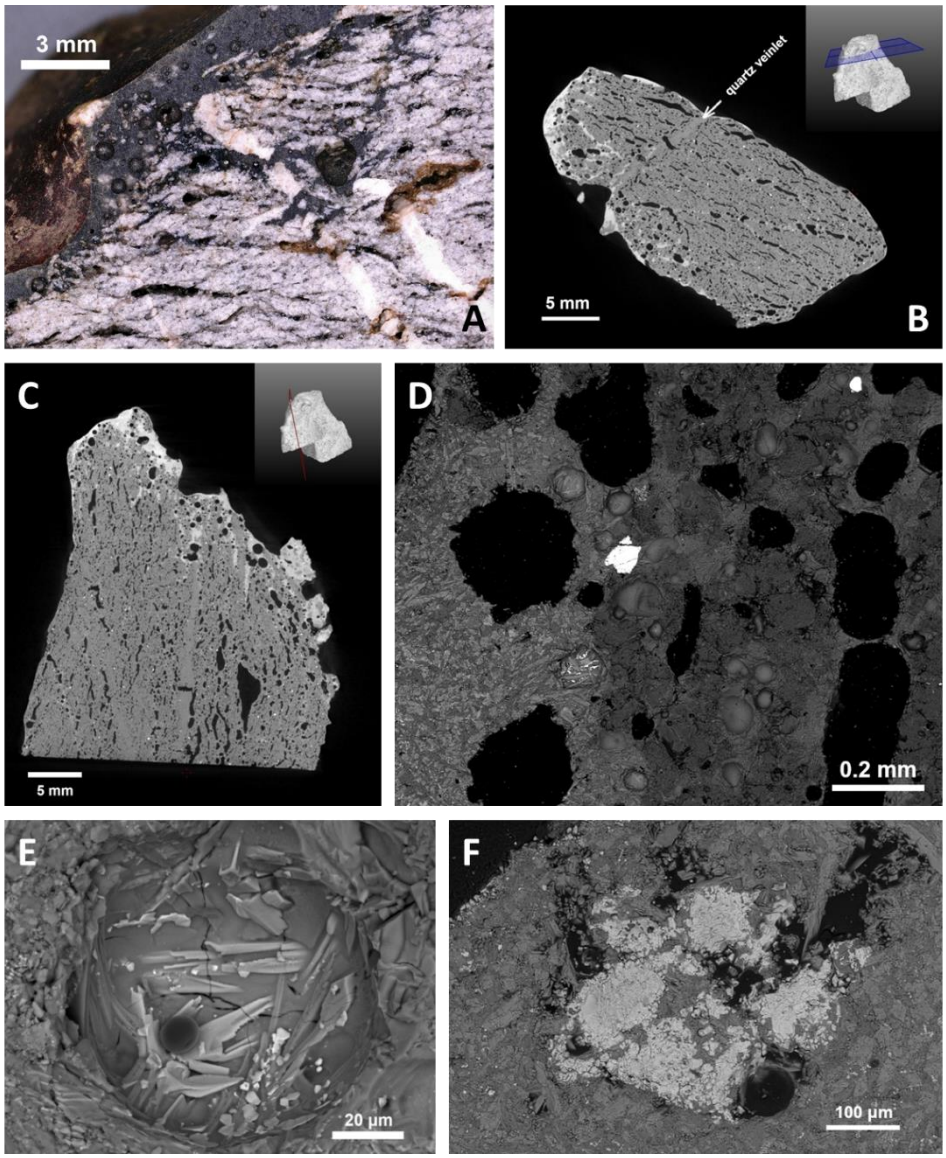

Figure 33. Injection of dark melt into a quartzite pebble (Crater No. 4, #16132). (**A**) Dark melt with isolated quartz remnants. (**B**,**C**) CT: the basic melt is bright; relatively undisturbed quartz veinlets partly act as barriers. (**D**) BSE image: basic melt (bright, on the left) with sharp boundary to the original rock (with gray quartz, a little brighter glass and bright zircon); the melt layer also contains cavities partly filled with crystals. (**E**) Crystals in a cavity (note the longitudinal grooves in the columnar crystals); a darker carbon sphere is possibly contamination (black in both transmitted and reflected light). (**F**) Crushed Fe-Mg-Ti oxide mineral (probably Mg-rich titanomagnetite).

In both craters at Emmerting, melt (regardless to its origin) also penetrated into fractures in individual mineral grains, mainly quartz and zircon (Figures 34 and 35), and solidified as a glass there. It follows that there was a pressure gradient, unless the melt viscosity was (unlikely) extremely low due to high temperature. The underpressure caused by rarefaction wave(s) may have led to suction of the surrounding melt. Note that zircon is also used in thermally resistant materials and its intense fracturing due to temperature changes alone is unlikely.

 doi:10.20944/preprints202403.1373.v1

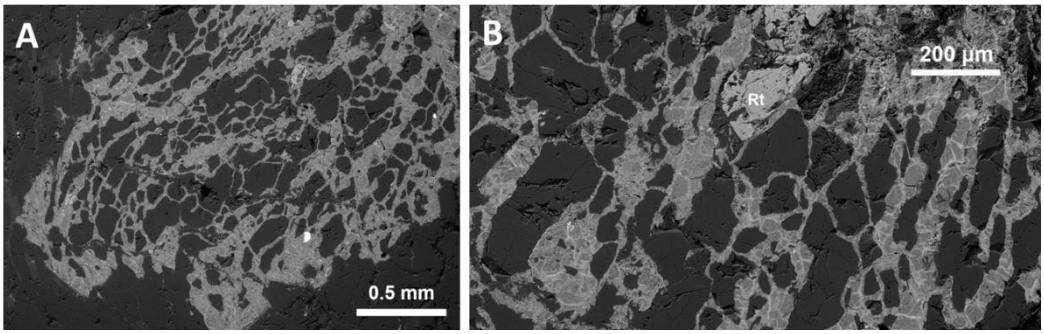

Figure 34. Melt penetrations in quartzitic rock (Crater No. 5, #5/1/0a; BSE images). (**A**) Injections of melt chemically similar to a mafic silicate (chlorite, tourmaline or amphibole, containing Al, Fe, Mg, Na and little Ca) into fractured quartz. (**B**) Detail of other injected quartz (dark gray); Rt – rutile, possibly deformed; the melt separated into very fine, usually acicular Fe-oxides (bright) and silicate glass (medium gray), also crystallization of fine cristobalite is possible.

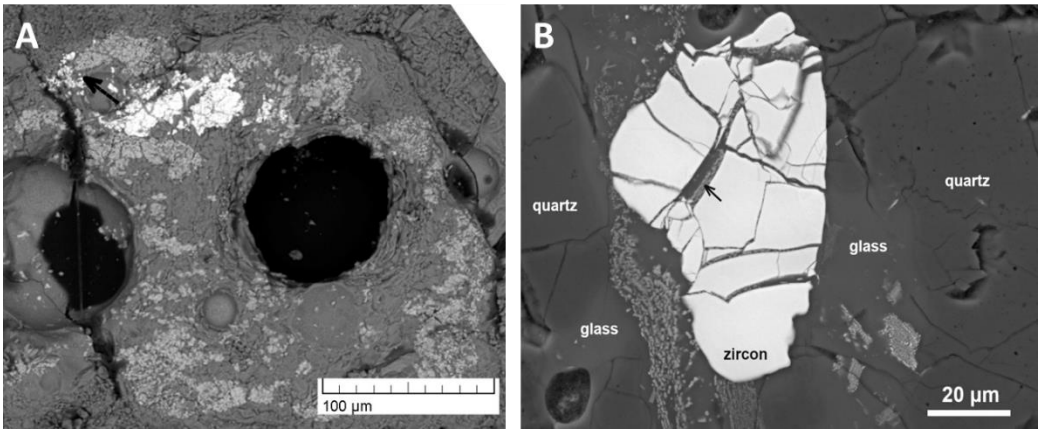

Figure 35. Melt penetration into zircon (BSE images). (**A**) Zircon (white) and TiO_2 phase (rutile?, light gray) in glass of K-feldspar composition (Crater No. 4, #16133); the zircon had been probably a single crystal whose part was shifted away by an expanding bubble (arrow). (**B**) Zircon with many fractures penetrated by melt, which usually differentiated into silicate glass (dark) and very tiny Fe-Al oxide crystals (gray; see an arrow), similar to the surrounding glass, where Ti(-Fe) oxides also crystallized (Crater No. 5, #5/1/0a).

4.3.7. Glass Melting Temperature

The sample tested (#16131, Crater No. 4; dark, probably biotite-derived melt) did not melt even at the maximum temperature (1500 °C). Softening (deformation) temperature was 1360 °C in the oxidizing atmosphere and 1380 °C in the reducing atmosphere.

4.4. Magnetometry

In both craters at Emmerting and in the Kaltenbach structure, MS is generally high. In carbonates, however, it forms two distinct groups with values < 0.20 × 10^{-3} SI and > 0.40 × 10^{-3} SI, with maxima almost 2.6 × 10^{-3} SI (see Tables A3 and A6). All silicate pebbles and ca. half of the vein quartz samples have mean MS > 0.25 × 10^{-3} SI, with peak values exceeding 10^{-2} SI in individual measurements (the most magnetic sample, except for the problematic #121, is #418 from Crater No. 4 with range of 7.0 to 11.3 × 10^{-3} SI).

In limekilns, primary carbonates were not sampled. The silicate rocks which experienced melting usually have high MS (the most magnetic sample is Ko-007 with 3.5 to 15.4 × 10^{-3} SI – Table A6) but it is not a rule, and values < 0.10 × 10^{-3} SI also appear (e.g., Ko-003), in contrast to the craters at Emmerting. As the high MS may relate to high temperature, it can mean that in craters the peak temperature was even higher.

 doi:10.20944/preprints202403.1373.v1

Thermo-remanent magnetization measurements (two samples from Kaltenbach structure and one from Crater No. 5) show spatially relatively homogeneous magnetization (G. Kletetschka et al., unpublished data), which is unlikely to be caused by lightning.

4.5. Disequilibrium Character of Melting and Evaporation, and Its Implications

All three binary eutectic points for melting of K-feldspar, quartz and albite are well below 1100 °C while individual feldspars melt above this temperature (e.g., [29]), and quartz (metastable or transformed to cristobalite) above 1700 °C. Eutectic melting of albite and K-feldspar is likely in the sample #123 (Kaltenbach), i.e., in highly acidic orthogneiss where mixed alkali feldspar (microperthite?) was probably present. Quartz was very little involved in melting; more likely it was partially dissolved in melt locally. With the possible exception of tiny unspecified oxide phases (#123, #420), we found no minerals which could be products of incongruent melting of primary minerals (e.g., sillimanite or cordierite from micas/chlorite; mullite from micas, clay minerals or feldspars). We also have not observed primary cristobalite which should be formed from quartz prior to melting during equilibrium heating (in the presence of mineralizers, especially alkalis, also tridymite could form). Both tridymite and cristobalite, also mentioned by [10] from Crater No. 4, probably crystallized from highly viscous cooling melt. Tridymite dendrites (even macroscopic) on the surface of the sample #421 (and possibly #407) resemble those occurring as product of devitrification in industrial glasses [25].

The peak temperature in craters is delimited by several indices: total melting of individual feldspars and large-scale melting of micas prove that the value 1100 °C was exceeded commonly. Experimental melting of separated glass indicates temperature greater than 1500 °C which, however, could be influenced by previous devolatilization and magnetite crystallization from melt, not excluding the possibility that the melt formed from mica at a lower temperature. The fact that quartz mostly did not melt and zircon was not decomposed limits the temperature to ca. 1700 °C and (at most) 1800 °C, respectively [25,27]. Thus, maximum temperature estimate around 1600 °C in most of melted pebbles seems to be reasonable. However, the strongly expanded pebble (see Figure 15) requires a higher temperature, as in this case feldspars should have not only melted but also evaporated, and quartz (at least partly) melted too.

The expansion of feldspar glass may have been caused by two factors: dehydration of secondary minerals, like kaolinite and muscovite-illite, or evaporation of the feldspathic melt itself. Note that heating and dehydration of clay minerals at atmospheric pressure leads to formation of mullite, a thermally resistant mineral which, however, was not observed even in large pores. The evaporation of feldspathic melt at temperatures lower than necessary for melting of quartz may be consequence of under-pressure after the pressure wave rebound.

The external heat supply was limited, as evidenced by very thin surface glass layers. This also implies that the fire of organic matter, though proved (see charred moss in Figure 23B), could not be the decisive factor. A question arises how the intensive melting, expansion, and even partial evaporation of silicate melt could happen inside the pebbles from the craters.

We suggest (see also [12]) that sudden melting in the strongly deformed rocks was caused by the pressure wave and subsequent decompression when more compressible (i.e., relatively soft and/or porous) matter, like weathered micas or feldspars, melts preferentially, while eutectic melting (e.g., quartz with feldspars) is very limited; shock pressure of tens of GPa is needed for the "one-shot" melting ([27] and references therein). The key role of decompression due to rebound of target rocks and minerals after the compression phase for impact-induced melting is well known (e.g., [30]). We have not observed evidence for shock pressure greater than ca. 8 GPa, nevertheless, we do not exclude that it can be found (PDF and spallation were mentioned in [23]). Note that PDF or any other shock phenomena have not been found even in much larger confirmed impact craters (e.g., in the Odessa, Henbury, and Morasko strewn fields) [9].

It is well known that the formation of PDF is dominant in compact rock massifs, while in a porous environment, it is relatively suppressed; note that coarse fluvial terraces and moraines have incomparably larger void space than the porous rocks investigated in confirmed impact craters, like

 doi:10.20944/preprints202403.1373.v1

sandstones [31]. The effect of groundwater could also be significant [13]. The impacts into targets dominated by large pebbles are little understood yet. It can be expected that the temperature effects will be dominant, while looking for shock pressure effects like PDF in quartz could be little productive. Partly similar substrate rich in up to almost meter-sized coarse clasts (mainly of basalt) was documented in the Bajada del Diablo strewn field, Argentina, but few information about mineralogy, chemistry and deformation from these craters has been published [32].

The transformation of shock- and other pressure waves to heat could be repeated several times due to collisions of individual pebbles. Another factor is underpressure during passage of the rarefaction wave which could help to melt expansion and partial evaporation. The stones heated inside may have cooled slowly even without an external heat source. Stones ejected away from the craters did not melt, because they underwent only one or few collisions.

Secondary projectiles accelerated by the impactor explosion are not well documented in literature, but they should be significant in the case of impact into target dominated by large pebbles or boulders. A stone with several meters in size and several tons in weight was described which formed a furrow in the permafrost near the epicenter of the Tunguska explosion [33]. The boulder, formed by sandstone (or conglomerate), as well as its fragments collected in soil, was partly coated with thin glass. The authors [33] calculated that the stone had to hit the ground with a velocity higher than 500 m/s (they suggested that it could represent a new type of meteorite, which however is inconsistent with its chemical and isotopic composition [34]). Therefore, that stone may represent a secondary projectile. Smaller stones may have been accelerated to much higher velocity. Fehr et al. [7] also documented probable effects of secondary projectiles, but with a low velocity, in the vicinity of several craters near Emmerting. Theory, experiments and morphology of craters on some asteroids suggest that in highly porous target the ejecta formation is strongly suppressed in favor of compaction of the underlying sediments [35]. Therefore, collisions of particles within the crater should be more common.

In ejecta of the Carancas crater with a diameter similar to craters at Emmerting, only microscopic melting of the target material has been found. On the other hand, weak shock effects in quartz and possibly in feldspar were observed, requiring pressure of at least 5, possibly 10 GPa [36]. As shown experimentally, shock pressure of 5 GPa is sufficient for local melting in a dry sandstone [37]. It can be inferred that in coarse-grained sediments at Emmerting, the portion of impact energy transformed to heat was greater than at the Carancas impact, and probably greater than in experiments in [37].

4.6. Decarbonization in Craters

Limestone pebbles in the Alpine foreland may have conspicuous morphology and structures due to dissolution in acidic soils and formation of corrosion layers ([38] and references therein). We observed weathering crusts, representing corrosion layers, mainly in Crater No. 4. Freude [38] investigated these phenomena in the surroundings of Grabenstätt, and did not present anything similar to the probably decarbonized, i.e., expanded or chalk-like, surfaces (Figures 19–21); he did not investigate the Kaltenbach structure, however.

The reactive Ca-rich phases were not artificially removed from craters, and their subsequent hydration was an important heat source. While it probably did not produce temperatures significantly exceeding 100 °C, it efficiently removed liquid water, probably enabling the fire of organic matter to persist until all combustible was exhausted.

4.7. Composition of Glasses

Chemical composition of the glass was previously documented with many EMP analyses in Crater No. 4 [23] and in the Kaltenbach structure [17]. The paper [17] reports a high content of K_2O (up to 16 wt.%, similar to our results from Emmerting), but locally also SiO_2 (up to 96 wt.%, the top values testify for temperatures exceeding 1600 °C, unless additional volatile components not measurable by EMP were present). In many pebbles of the Kaltenbach structure, “internal” glasses formed from Al-rich minerals (micas, their alteration products, and feldspars) and more siliceous

 doi:10.20944/preprints202403.1373.v1

surface glasses were distinguished [17]. Feldspar-derived glasses and transitions between feldspar and glass were also observed within pebbles of Crater No. 4 [23].

The two elements most enriched in the surface glasses of Crater No. 4, namely K (similar to Rb) and Cu, are known from cosmochemistry to be moderately volatile and characterized by significant evaporative loss from material of approximately chondritic composition (e.g., [39,40]). However, no systematic depletion in K of the melts from dozens of terrestrial impact craters (including strongly expanded pumice glasses) can be inferred (e.g., [30,41], and references therein); there are few data on Cu. Tektites very likely experienced volatile loss of Cu (together with Zn, Sb, etc.), but content of K in moldavites (together with Rb and Cs) is relatively high, making its significant volatilization doubtful (e.g., [42]).

The probably biotite-derived dark porous melt in sample #421 is remarkably poor in K (see Table 2), which makes the question of evaporative fractionation relevant. A role of volatile loss is also supported with preferential crystallization of magnetite at the walls of pores. Occurrence of Fe-Al spinels prevalently near the pores was also observed in medieval ceramics burnt to ca. 1250 °C [43]. However, influence of volatiles from interior melt on the surface glasses (which are older) is doubtful. In any case, volatilization of melts derived from individual minerals can be important after shock heating. Note that alkalis can evaporate in the form of clusters (e.g., alkali oxide together with equal molar amount of alumina and silica), as shown in experiments with feldspars [44]. This could explain why Al-rich glasses are not common (Table 2) even in melts obviously derived from micas, or from micas and feldspars. Disequilibrium heating of micas, however, has been poorly experimentally constrained. Shock heating of muscovite in a plasma torch lead to expansion and significant depletion in K (M. Faltus, unpublished data).

The elements concentrated in surface glasses (K, Cu, partly Zn, Rb) are also typical for plant biomass ash. Also relatively high contents of Ca, Mg, and occasionally Mn in glass coatings on rocks poor in these elements could be influenced by plant biomass. In wood biomass and ash, Ca usually strongly prevails over K, but K_2O content can be greater than that of CaO in the ash from green biomass, like grasses, moss, ferns, and the foliage of woody species [45–48]. Origin from terrestrial biomass is improbable for SiO_2 (only grasses and ferns could make a relevant contribution) and Na_2O. Silica more likely originates from overlying humus, whose composition is strongly influenced by atmospheric deposition and little dependent on bedrock; it also naturally concentrates several metals like Cu [46,48]. Therefore, a natural mixture of humus, green biomass and leaf litter (poor in Al) is the most probable source of the biogenic material in craters.

Foliage of trees and shrubs could be ignited by thermal radiation of the impactor and torn down by pressure wave, and so the body could push the gas/aerosol enriched in biogenic elements in front. Biomass ignition at the earliest stage of the impact, producing K and Ca carbonate (promptly reacting with silica), has also been considered for moldavite tektites [42,49]. In places, the biomass ash (perhaps dissolved in a supercritical aqueous fluid – see [13]) or possibly gas condensate mixed with the melt formed in the pebbles or on their surface, producing glass layers of different compositions. Concentration of K, Cu, and Na (only locally Zn) suggests a condensation or precipitation of moderately volatile components (see e.g., [50]) on relatively cold surface of pebbles; we can speculate that highly volatile elements like S, Cl, and partly Zn escaped in fluid after external pressure decrease. Gamma-ray spectrometry as well as chemical data [13] show that the geological environment in which all the structures investigated here formed is poor in the elements most enriched in glass coatings (K, Cu, Rb). Another proof of the "external" supply of K is its concentration in glass on various pebbles, including those poor in K.

Ernstson et al. [8] suggested that relatively homogeneous glass may be formed by melting of clay (as imitated by experimental heating of wet clay to 2500 °C for few seconds), which, however, is little consistent with low Al content and high K content of glass coatings.

The surface glasses from limekilns where influence of biomass ash is inevitable are also rich in K, Cu, and (relatively to the biomass) in Na, and poor in Ca. This excludes that they would represent simply molten ash prevalently of wood (including some green biomass). Volatility of alkalis and Cu may have been a key factor. Highly reactive forms of alkali metals reacted with the original surfaces,

 doi:10.20944/preprints202403.1373.v1

forming silicate glass (similar to energetic devices burning K-rich biomass; e.g., [51]). Contribution of spruce needles to concentration of K, Cu, and possibly slightly Ni is also probable. Again, more volatile metals like Zn could have been intensely lost and thus not significantly concentrated.

4.8. Origin of the Kaltenbach Structure: Crater or Limekiln?

None of the closely investigated samples from the craters at Emmerting displays zonal melting which would allow comparison to materials exposed for relatively long time to man-made fire. Instead, we observed only thin surface glass there, or some minerals melted in the whole pebble's volume, or combination of both (see also Table A3). A sample melted from one side was found in the Kaltenbach structure; also its morphology and mineralogy are somewhat special, resembling a volcanic rock, which could represent material brought by humans (Figure 36A). In addition, another, rather flat and sharp-edged fragment from the Kaltenbach structure could represent a roofing material or brick (Figure 36B; it has also the highest MS of all samples: mean 20.4 × 10^{-3} SI). However, the material was picked-up several times and there were many opportunities for contamination, including waste dumping into the natural depression.

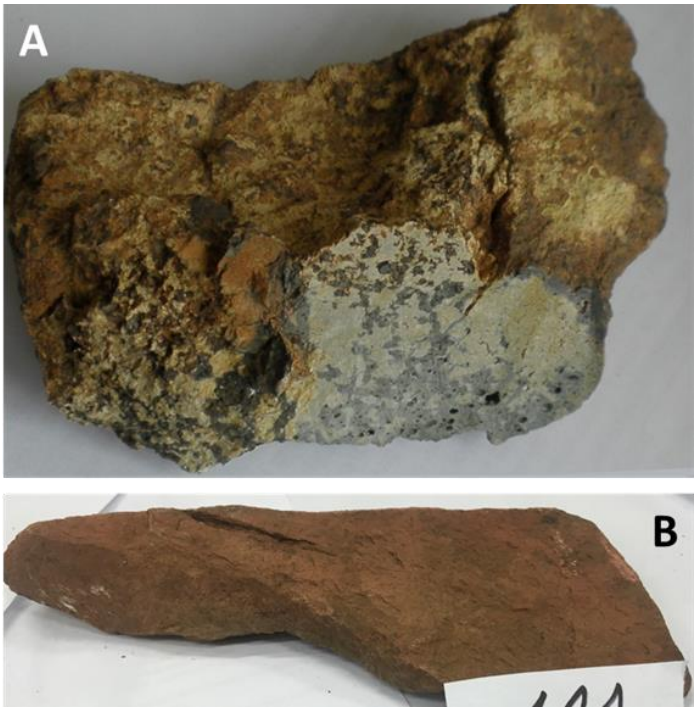

Figure 36. "Exotic" rocks found at the Kaltenbach structure. (**A**) Possibly volcanic, one-side re-melted rock with sphene (pink to orange) (#125; sample length 9 cm). (**B**) Meta-siltstone, or brick or similar material (#121; sample length 13 cm).

The superparamagnetism (most likely caused by nanoparticles) of stones from both Crater No. 4 and Kaltenbach structure has been interpreted as consequence of very short heating [52]. Nevertheless in limestones, the nanoparticles may also simply reflect submicroscopic grain size of the original iron hydroxides / hydrated oxides.

The morphology corresponds to an impact crater, not a limekiln. However, the owners may have partly recultivated and hidden their limekilns after usage to escape taxation.

4.9. Other Anthropogenic Processes

Many human activities are able to cause disequilibrium melting. For example, man-made fires partially melted walls of many pre-historic to early mediaeval hillforts in Europe, forming so-called vitrified forts, especially in Scotland. Stones in these walls, however, had been intercalated with wood and possibly other combustibles (see also [53]). Such arrangement is impossible to imagine in the

 doi:10.20944/preprints202403.1373.v1

depressions investigated. Some authors [54] suggested relatively low temperatures (< 900 °C) as sufficient for vitrification of the walls but they assumed eutectic melting of biotite and quartz, i.e., a long-lasting equilibrium process.

The Crater No. 5 is located in poorly drained and frequently wet environment quite unsuitable for any device demanding for firing. It was not better in the past due to proximity of fossil side channels of the Alz river, as displayed in a historical map [3].

Regarding slags from old iron metallurgy, the ore was always processed near the deposits exploited [55]. The only relevant resources in the region are sedimentary ores (see also [56]). Thus the slags should have similar composition to those from Grubet near Aichach [55]. These slags have high content of total Fe (> 30 wt.%) and Mn (6.5 wt.% MnO) and are dominated by Fe silicates. This is incomparable to composition of any Fe-rich matter we observed. Slags usually contain metallic phases and/or sulfides, which have not been found in our samples, and they are usually very rich in Fe and/or Ca (e.g., [57]). In addition, some stones seemingly similar to slags have preserved original calcite or quartz veinlets from the rock, and even original layering (see Figure 37). Finally, no burnt fine-grained material, like clay or loam, which would be necessary for the furnace construction, has been found in the craters (contrary to limekilns).

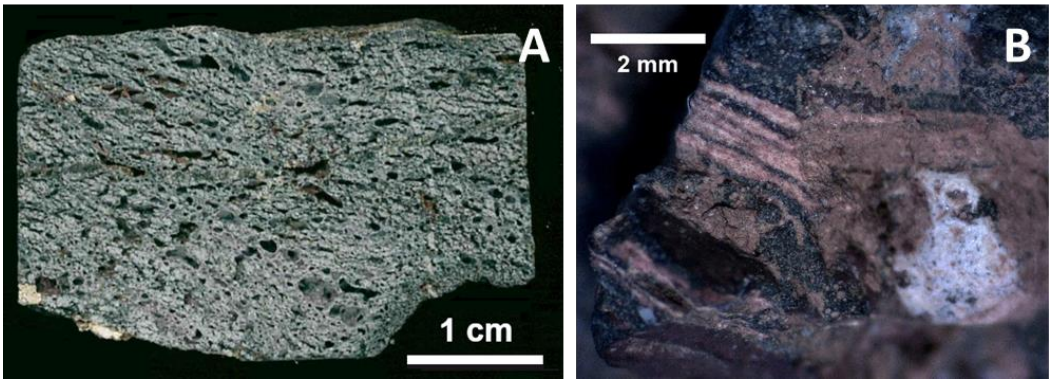

Figure 37. Melting-affected natural rocks partly similar to metallurgic slags. (**A**) Almost completely melted and expanded basic rock (Crater No. 4, #419); note the quartz(?) veinlet crossing the whole specimen on the right which is partly disturbed by the expansion. (**B**) Preserved relics of layering of the original sedimentary rock (Kaltenbach, #124).

4.10. Possible Convergence of Impact and Anthropogenic Processes

Rappenglück et al. [18] suggested that the "Chiemgau Impact" affected various anthropogenic products such as metallic objects. This would allow coincidence of impact-related phenomena and artifacts at the same sites. However, the authors have not presented any comparison with a "background material", i.e., definitively not shock-affected. In our opinion, their statements rely too much on the assumption of "ubiquitous" effects of the "Chiemgau Impact" in the area. Drastic effects of airbursts (possibly accompanied by small impacts) in a densely populated area, including destruction of buildings and melting and deformation of various objects, have been documented in Tall Hammam (and more Bronze-Age archaeological sites) in Jordan [58]. The opposite – the crater as a natural depression used by humans – may, however, be more likely in the area of Emmerting. Fehr et al. [7] suggested secondary utilization of Crater No. 5 as a limekiln, but neither presented nor cited any evidence for that. We consider this possibility highly unlikely (see above), although some anthropogenic influence cannot be excluded without uncovering and archaeological research. The role of natural and anthropogenic processes in formation of the Kaltenbach structure remains open.

5. Conclusions

In the craters No. 4 and 5 at Emmerting, three major processes are documented:

1. Deposition of hot material which solidified to glass (usually thin and transparent), or reacted with carbonate to form expanded "pumice", on the surface of pebbles (usually not on the whole

 doi:10.20944/preprints202403.1373.v1

surface – typically the bottom side was sheltered). The surface glass coatings may have started to form by thermal wave shortly before the impact.

2. Ductile deformation of variable intensity (with limited fragile deformation but intense fracturing of mineral grains), using older as well as newly formed discontinuities; in some cases this deformation had to be associated with extreme strain, excluding explanation by any realistically possible human activity. The ductile character of the deformation points to a high temperature, which however did not always cause melting.
3. Solidification of melts formed inside the pebbles or from secondary projectiles. These melts, despite being far from equilibrium, were also able to fill even thin fractures in individual mineral grains (perhaps owing to underpressure during rebound of the compressed rock); expansion of gases also lead to extrusions and formation of miniature "cinder cones" on the surface of some pebbles. The role of under-pressure in melt evaporation is also possible.

We have observed no evidence that the pressure would reach values usually cited as necessary for "one-shot" melting by the shock wave (tens of GPa). Nevertheless, the large void space between individual pebbles and repeated mutual collisions of pebbles after the impact and explosion of the impactor in a coarse unconsolidated target support melting and lead to complicated relations between melting and deformation. Classical shock effects like PDF in quartz develop in such targets only at a pressure greater than necessary for significant melting, which is another reason why they are, in general, rarely found in small craters.

The character of melts in most samples from craters proves quick heating with minimum of eutectic melting. Typical highly porous "internal" melt formed likely from micas (like chloritized biotite) and it is rich in secondary Fe, Al, and Ti oxide minerals. Feldspars melted in many samples and they formed mixed alkali-feldspar glass, and even glass pseudomorphs after K-feldspar and albite without any eutectic reaction. The feldspar-derived glasses contain abundant bubbles, and the presence of a strongly expanded Ca-poor pebble points to evaporation of silicates in Crater No. 4. Only in few samples where high temperature persisted longer (mainly at the bottom of Crater No. 4), quartz was a little dissolved at grain boundaries. Minerals, usually microscopic, crystallized from melt in places.

In limekilns, time was also usually insufficient for equilibrium melting. However, the thermal transformation was more static, enabling formation of thick glass layers and growth of droplets. Limited deformation dominated by a gravity effect is characteristic, burnt loam is common (typically with imprints of spruce twigs with needles), and charcoal can be found. Stones from limekilns also tend to have more regular shapes. Relatively large pieces of partly re-carbonized lime are found. In contrast, such decarbonization phenomena which are limited to the surface of stones are typical for craters.

Enrichment in K and Cu of surface glasses on pebbles from limekilns comes from biomass ash, with preferential concentration of moderately volatile elements. Similarly, composition of thin K-rich glasses on surface of pebbles from both craters at Emmerting indicates their "external" origin and influence of plant-derived material. Influence of the meteoritic contamination on the elements analyzed in glass coatings in craters is not significant.

In the Kaltenbach structure, some anthropogenic contamination is probable (however, possibly long time after the depression's formation). Deformation likely related to the event of interest is limited to some fracturing of pebbles and deformation of partially molten rocks, dominated by gravity and gas expansion (nevertheless, strongly disequilibrium melting and complete filling of fractures by glass are remarkable in some cases).

Several samples from craters as well as limekilns may macroscopically resemble metallurgical slags, but their composition and relics of original rock's textures, including quartz and calcite veinlets, exclude such comparison.

Regardless of the meteoritic contamination found only in the Crater No. 4 so far, we believe that the high-temperature effects and deformation documented would be sufficient evidence for impact origin of both the craters at Emmerting. Our results can be used in research of similar craters, as the search for microscopic meteorite fragments or ultratrace chemical contamination is time- and cost-

demanding; the evidence may be even completely lost (due to weathering of the meteoritic matter, or chemically indistinct impactor like a comet).

Supplementary Materials: The following supporting information can be downloaded at the website of this paper posted on Preprints.org, Figures A1-A4: Photographs of selected studied sites; Table A1: XRF analyses of samples from limekilns; Table A2: EMP analyses of samples from limekilns; Table A3: Overview of the first set of samples from Crater No. 4; Table A4: Mineralogy of samples from craters and the Kaltenbach structure; Table A5: XRF analyses of samples from craters and the Kaltenbach structure; Table A6: Magnetic susceptibility.

Author Contributions: Conceptualization, V.P., P.K. and H.H.; methodology, V.P., P.M., H.H. and T.T.; investigation, V.P., H.H., P.K., L.T., P.M., T.T., J.A. and K.S.; resources, H.H., V.P., P.K. and L.T.; data curation, V.P. and J.M.; writing—original draft preparation, V.P., P.K. and G.K.; writing—review and editing, V.P., J.M. and G.K.; visualization, V.P., J.A. and J.M.; supervision, V.P.; project administration, V.P.; funding acquisition, T.T., K.S. and J.M. All authors have read and agreed to the published version of the manuscript.

Funding: The work was funded by the Ministry of Education, Youth and Sports of the Czech Republic within the projects LM2023073 (The VR-1 Nuclear Experimental Hub) and RVO: 68145535 (project for the long-term conceptual development of research organizations at the Institute of Geonics).

Data Availability Statement: The data presented in the tables and figures or elsewhere are openly available as the Supplementary Materials or on request from the corresponding author.

Acknowledgments: The authors thank the Chiemgau Impact Research Team, namely Barbara and Michael Rappenglück, Hans-Peter Matheisl, and Ernst A. Neugebauer for their assistance in the field measurements and sample collection at Emmerting and Grabenstätt. They also thank M. Faltus for valuable discussions.

Conflicts of Interest: The authors declare no conflict of interest.

References

1. Kos, P. Research of High Middle Ages lime kilns in the south part of the Moravian Karst in consideration of Mokrá Village region. *Archeol. Tech.* **2005**, *26*, 27–68. In Czech, available online: http://archeologiatechnica.cz/sites/default/files/2018-04/Kos%2027_68.pdf (accessed on 17 October 2023).
2. Herrmann, H. Kalkbrandstellen in der Eiszerfallandschaft südlich und westlich von Seeshaupt. Bernried am Starnberger See, Germany, 2021.
3. BayernAtlas. Landesamt für Digitalisierung, Breitband und Vermessung, München. Available online: https://atlas.bayern.de (accessed on 17 October 2023).
4. Geologische Karte von Bayern 1:500.000, 4. Auflage. Bayerisches Geologisches Landesamt, München, Germany, 1996.
5. Válek, J.; van Halem, E.; Viani, A.; Pérez-Estébanez, M.; Ševčík, R.; Šašek, P. Determination of optimal burning temperature ranges for production of natural hydraulic limes. *Constr. Build. Mater.* **2014**, *66*, 771–780. https://doi.org/10.1016/j.conbuildmat.2014.06.015
6. Rappenglück, M.A.; Ernstson, K.; Mayer, W.; Beer, R.; Benske, G.; Siegl, C., Sporn, R.; Bliemetsrieder, T.; Schüssler, U. The Chiemgau impact event in the Celtic Period: evidence of a crater strewnfield and a cometary impactor containing presolar matter. Available online: https://www.chiemgau-impakt.de/pdfs/Chiemgau_impact.pdf (accessed on 17 October 2023).
7. Fehr, K.T.; Pohl, J.; Mayer, W.; Hochleitner, R.; Faßbinder, J.; Geiß, E.; Kerscher, Y. A meteorite impact crater field in eastern Bavaria? A preliminary report. *Meteorit. Planet. Sci.* **2005**, *40*, 187–194. https://doi.org/10.1111/j.1945-5100.2005.tb00374.x
8. Ernstsson, K.; Mayer, W.; Neumair, A.; Rappenglück, B.; Rappenglück, M.A.; Sudhaus, D.; Zeller, K.W. The Chiemgau crater strewn field: evidence of a Holocene large impact event in southeast Bavaria, Germany. *J. Sib. Fed. Univ. - Eng. Technol.* **2010**, *1*, 72–103. Available online: https://core.ac.uk/download/pdf/38633216.pdf (accessed on 17 October 2023).
9. Osinski, G.R.; et al. Impact Earth: A review of the terrestrial impact record. *Earth Sci. Rev.* **2022**, *232*, 104112. https://doi.org/10.1016/j.earscirev.2022.104112
10. Rösler, W.; Patzelt, A.; Hoffmann, V.; Raeymaekers, B. Characterization of a small crater-like structure in S.E. Bavaria, Germany. In Proceedings of the First International Conference on Impact Cratering in the Solar System, Noordwijk, Netherlands, 8-12 May 2006. Available online: https://sci.esa.int/documents/33321/35974/1567255423911-ESLAB40-Proc_295499-Roesler.pdf (accessed on 18 October 2023).
11. Procházka, V.; Martinec, P.; Štorc, R.; Kalenda, P.; Thinová, L.; Tengler, R.; Mizera, J. Holocene impact crater at Emmerting (Bavaria): mineralogy of the filling including meteorite and a possible explanation of the compact body below the crater bottom. In Proceedings of the 27th Quaternary Seminary Meeting, Brno,

Czech Republic, 2 December 2022. In Czech, available online: https://www.researchgate.net/publication/368358601 (accessed on 18 October 2023).
12. Procházka, V. Melt behavior in two impact craters at Emmerting, Germany: Deformation, expansion, injections, and the role of underpressure and mutual collisions of pebbles. In Proceedings of the 54th Lunar and Planetary Science Conference, The Woodlands, TX, USA, 13–17 March 2023. Available online: https://www.hou.usra.edu/meetings/lpsc2023/pdf/2102.pdf (accessed on 18 October 2023).
13. Procházka, V.; Kalenda, P.; Martinec, P.; Mizera, J.; Thinová, L.; Trojek, T.; Kletetschka, G.; Štorc, R.; Adámek, J.; Švanda, P. Meteoritic matter and spherules in a presumed impact crater at Emmerting, Germany. *Minerals* **2024** (to be submitted)
14. Van Husen, D. Die Ostalpen in den Eiszeiten; Geologische Bundesanstalt: Vienna, Austria: pp. 1–24. Available online: https://opac.geologie.ac.at/ais312/dokumente/Husen_1987_Eiszeiten_1.pdf (accessed on 18 October 2023).
15. Cicconi, M.R.; McCloy, J.S.; Neuville, D.R. Non-Magmatic glasses. *Rev. Mineral.* **2022**, *87*, 965–1014. https://doi.org/10.2138/rmg.2022.87.21
16. Kalenda, P.; Thinová, L.; Tengler, R.; Procházka, V.; Mizera, J.; Martinec, P.; Kletetschka, G.; Trojek, T. Two impact craters at Emmerting, Germany: Field documentation and geophysics. Geodynamics **2024** (in press).
17. Neumair, A.; Waitzinger, M.; Finger F. Interesting glass coatings on cobbles and rock fragments from the Alpine foreland, SE-Bavaria, Germany, and their possible origin. In Proceedings of GeoTirol2016 - Annual Meeting of DGGV (German Geological Society) and PANGEO Austria, 25-28. September 2016, Innsbruck, Austria, 25–28 September 2016. Available online: https://www.researchgate.net/publication/308674645 (accessed on 18 October 2023).
18. Rappenglück, B.; Hiltl, M.; Poßekel, J.; Rappenglück, M.A.; Ernstson, K. People experienced the prehistoric Chiemgau Meteorite Impact – Geoarchaeological evidence from Southeastern Germany: a Review. *Mediterr. Archaeol. Archaeom.* **2023**, *23*, 209–234. https://doi.org/10.5281/zenodo.7775798
19. Ernstson, K. The Digital Terrain Model (DTM) and the evaluation of known and the search for new craters in the Chiemgau meteorite impact strewn field. Chiemgau Impact Research Team, 2017. Available online: https://www.chiemgau-impakt.de/wp-content/uploads/2017/01/DGM-1-final-1.pdf (accessed on 18 October 2023).
20. Doppler, G.; Geiss, E. Der Tüttensee im Chiemgau - Toteiskessel statt Impaktkrater. Bayerisches Landesamt für Umwelt, 2005. Available online: https://www.lfu.bayern.de/geologie/meteorite/bayern/doc/tuettensee.pdf (accessed on 18 October 2023).
21. Huber, R.; Darga, R.; Lauterbach, H. Der späteiszeitliche Tüttensee-Komplex als Ergebnis der Abschmelzgeschichte am Ostrand des Chiemsee-Gletschers und sein Bezug zum " Chiemgau Impakt " (Landkreis Traunstein, Oberbayern). *E&G Quaternary Sci. J.* **2020**, *69*, 93–120. https://doi.org/10.5194/egqsj-69-93-2020
22. Rösch, M.; Friedmann, A.; Rieckhoff, S.; Stojakowits, P.; Sudhaus, D. A Late Würmian and Holocene pollen profile from Tüttensee, Upper Bavaria, as evidence of 15 Millennia of landscape history in the Chiemsee glacier region. *Acta Palaeobot.* **2021**, *61*, 136–147. https://doi.org/10.35535/acpa-2021-0008
23. Schüssler, U. Chiemgau-Impakt: Petrographie und Geochemie von Geröllen mit Deformationsmerkmalen und starker thermischer Beanspruchung aus dem nördlichen Bereich des Impakt-Areals. Chiemgau Impact Research Team, 2005. Available online: http://www.chiemgau-impact.com/wp-content/uploads/2011/08/Petrographie-und-Geochemie.pdf (accessed on 18 October 2023).
24. Neumair, A.; Ernstson, K. Geomagnetic and morphological signature of small crateriform structures in the Alpine Foreland, Southeast Germany. In Proceedings of the American Geophysical Union Fall Meeting 2011, 5–12 December 2011, San Francisco, CA, USA. Available online: https://www.academia.edu/2643037 (accessed on 18 October 2023).
25. Bartuška, M. *Vady skla (Glass defects)*; Práh: Prague, Czech Republic; 606 pp.
26. Knobloch, V.; Knoblochová, Z.; Kučera, J.; Tláskal, J.; Urbanec, Z. Lechatelierite inclusions in moldavites and lechatelierite fragments in host sediments. In Proceedings of the 2nd International Conference on Natural Glasses, Prague, Czech Republic, 21–23 September 1987.
27. French, B.M. Traces of catastrophe. *A Handbook of Shock-Metamorphic Effects in Terrestrial Meteorite Impact Structures. LPI Contribution 954;* Lunar and Planetary Institute: Houston, TX, USA, 1998; 120 pp. Available online: https://ntrs.nasa.gov/citations/19990071201
28. Procházka, V.; Trojek, T. XRF- and EMP- investigation of glass coatings and melted domains of pebbles from craters in Chiemgau, Germany. In Proceedings of the 48th Lunar and Planetary Science Conference, The Woodlands, TX, USA, 20–24 March 2017. Available online: https://www.hou.usra.edu/meetings/lpsc2017/pdf/2401.pdf (accessed on 18 October 2023).
29. Schairer, J.F.; Bowen N.L. The system K_2O-$A1_2O_3$-SiO_2. *Am. J. Sci.* **1955**, *253*, 681–746.
30. Dressler, B.O.; Reimold, W.U. Terrestrial impact melt rocks and glasses. *Earth Sci. Rev.* **2001**, *56*, 205–284. https://doi.org/10.1016/S0012-8252(01)00064-2

31. Kiefer, S.W. Shock metamorphism of the Coconino Sandstone at Meteor Crater, Arizona. *J. Geophys. Res.* **1971**, *76*, 5449–5473. https://doi.org/10.1029/JB076i023p05449
32. Acevedo, R.D.; et al. The Bajada del Diablo astrobleme-strewn field, central Patagonia, Argentina: Extending the exploration to surrounding areas. *Geomorphology* **2012**, *169–170*, 151–164. https://doi.org/10.1016/j.geomorph.2012.04.020
33. Anfinogenov, J.; Budaeva, L.; Kuznetsov, D.; Anfinogenova, Y. John's Stone: A possible fragment of the 1908 Tunguska meteorite. *Icarus* **2014**, *243*, 139–147. https://doi.org/10.1016/j.icarus.2014.09.006
34. Haack, H.; Greenwood, R.C.; Busemann, H. Comment on "John's stone: A possible fragment of the 1908 Tunguska meteorite" (Anfinogenov et al., 2014, Icarus 243, 139–147). *Icarus* **2016**, *265*, 238–240. https://doi.org/10.1016/j.icarus.2015.09.018
35. Housen, K.R.; Sweet, W.J.; Holsapple, K.A. Impacts into porous asteroids. *Icarus* **2018**, 300, 72–96. http://dx.doi.org/10.1016/j.icarus.2017.08.019
36. Harris, R.S.; Schultz, P.H.; Tancredi, G.; Ishitsuka, J. Preliminary petrologic analysis of impact deformation in the Carancas (Peru) cratering event. In Proceedings of the 39th Lunar and Planetary Science Conference. League City, TX, USA, 10–14 March 2008. Available online: https://www.lpi.usra.edu/meetings/lpsc2008/pdf/2446.pdf (accessed on 17 March 2024).
37. Kowitz, A.; Güldemeister, N.; Reimold, W.U.; Schmitt, R.T.; Wünnemann, K. Diaplectic quartz glass and SiO_2 melt experimentally generated at only 5 GPa shock pressure in porous sandstone: laboratory observations and meso-scale numerical modeling. *Earth Planet. Sci. Lett.* **2013**, *384*, 17–26. https://doi.org/10.1016/j.epsl.2013.09.021
38. Freude, F. Strukturgeologisch-petrographische Untersuchungen an Karbonatgeröllen einer Schotterterrasse im Chiemgau und Diskussion der Ergebnisse im Rahmen der Impakt-Streufeld-Hypothese. Master Thesis, Friedrich-Alexander-Universität, Erlangen-Nürnberg, Germany, 2007.
39. Neuman, M.; Holzheid, A.; Lodders, K.; Fegley, B.; Jolliff, B.; Koefoed, P.; Chen, H.; Wang, K. High temperature evaporation and isotopic fractionation of K and Cu. *Geochim. Cosmochim. Ac.* **2021**, *316*, 1–20. https://doi.org/10.1016/j.gca.2021.09.035
40. Dauphas, N.; Nie, N.X.; Blanchard, M.; Zhang, Z.J.; Zeng, H.; Hu, J.Y.; Meheut, M.; Visscher, C.; Canup, R.; Hopp, T. The extent, nature, and origin of K and Rb depletions and isotopic fractionations in Earth, the Moon, and other planetary bodies. *Planet. Sci. J.* **2022**, *3*, 29. https://doi.org/10.3847/PSJ/ac2e09
41. Feldman, V.I. *Petrology of Impactites* (in Russian); Moscow University Press: Moscow, Russia, 1990; 297 pp.
42. Mizera, J.; Řanda Z. Geochemical indicators of biogenic component in source materials of moldavites. In *In the Footsteps of Warren B. Hamilton: New Ideas in Earth Science*; Foulger, G.R.; Hamilton, L.C.; Jurdy, D.M.; Stein, C.A.; Howard, K.A.; Stein, S., Eds.; Geological Society of America: Boulder, CO, USA, 2022; GSA Special Paper 553, ch. 26, pp. 335–346. https://doi.org/10.1130/2021.2553(26)
43. Gregerová, M.; et al. *Petroarchaeology of Ceramics in the Historical Past of Moravia and Silesia* (in Czech). Masaryk University: Brno, Czech Republic, 2010; 311 pp.
44. Gerasimov, M.V.; Dikov, Yu.P.; Yakovlev, O.I. New experimental evidence on cluster-type vaporization of feldspars. *Petrology* **2016**, *24*, 49–74. https://doi.org/10.1134/S0869591116010045
45. Vassilev, S.V.; Baxter, D.; Andersen, L.K.; Vassileva, C.G. An overview of the chemical composition of biomass: *Fuel* **2010**, *89*, 913–933. https://doi.org/10.1016/j.fuel.2009.10.022
46. Sucharová, J.; Suchara, I.; Holá, M.; Maříková, Š.; Reimann, C.; Boyd, R.; Filzmoser, P.; Englmaier, P. Top-/bottom-soil ratios and enrichment factors: What do they really show? *Appl. Geochem.* **2012**, *27*, 138–145. https://doi.org/10.1016/j.apgeochem.2011.09.025
47. Cílová, Z.; Woitsch, J. Potash – a key raw material of glass batch for Bohemian glasses from 14th–17th centuries? *J. Archaeol. Sci.* **2012**, *39*, 371–380. https://doi.org/10.1016/j.jas.2011.09.023
48. Tyler, G. Changes in the concentrations of major, minor and rare-earth elements during leaf senescence and decomposition in a Fagus sylvatica forest. *For. Ecol. Manag.* **2005**, *206*, 167–177. https://doi.org/10.1016/j.foreco.2004.10.065
49. Řanda, Z.; Mizera, J.; Frána, J.; Kučera, J. Geochemical characterization of moldavites from a new locality, the Cheb Basin, Czech Republic. *Meteorit. Planet. Sci.* **2008**, *43*, 461–477. https://doi.org/10.1111/j.1945-5100.2008.tb00666.x
50. Misra, M.K.; Ragland, K.W.; Baker, A.J. Wood ash composition as a function of furnace temperature. *Biomass Bioenergy* **1993**, *4*, 103–116. https://doi.org/10.1016/0961-9534(93)90032-Y
51. Jenkins, B.M.; Bakker, R.R.; Wei, J.B. On the properties of washed straw. *Biomass Bioenergy* **1996**, *10*, 177–200. https://doi.org/10.1016/0961-9534(95)00058-5
52. Procházka, V.; Kletetschka, G. Evidence for superparamagnetic nanoparticles in limestones from Chiemgau crater field, SE Germany. In Proceedings of the 47th Lunar and Planetary Science Conference, The Woodlands, TX, USA, 21–25 March 2016. Available online: https://www.hou.usra.edu/meetings/lpsc2016/pdf/2763.pdf (accessed on 20 October 2023).
53. Childe, V.G.; Thorneycroft, W. The experimental production of the phenomena distinctive of vitrified forts. *Proc. Soc. Antiq. Scot.* **1938**, 72, 44–55. https://doi.org/10.9750/PSAS.072.44.55

 doi:10.20944/preprints202403.1373.v1

54. Friend, C.; Dye, J.; Fowler, M. New field and geochemical evidence from vitrified forts in South Morar and Moidart, NW Scotland: further insight into melting and the process of vitrification. *J. Archaeol. Sci.* **2007**, *34*, 1685–1701. https://doi.org/10.1016/j.jas.2006.12.007
55. Strassburger, M.; Wieser, J. Early and high medieval iron production in the Grubet near Aichach. *Acta Rer. Natur.* **2014**, *16*, 33–50. Available online: https://actarerumnaturalium.cz/wp-content/uploads/2019/12/archiv_2014-16__02.pdf (accessed on 20 October 2023).
56. Langenscheidt, E.; Stahr, A. *Berchtesgadener Land und Chiemgau: Eine Geschichte von Bergen, Tälern und Seen*; Spektrum Akademischer Verlag: Heidelberg, Germany, 2011; 200 pp.
57. Piatak, N.; Ettler, V. *Metallurgical Slags: Environmental Geochemistry and Resource Potential*. Royal Society of Chemistry: Cambridge, UK, 2021; 305 pp.
58. Bunch, T.E.; et al. A Tunguska sized airburst destroyed Tall el Hammam a Middle Bronze Age city in the Jordan Valley near the Dead Sea. *Sci. Rep.* **2021**, *11*, 18632. https://doi.org/10.1038/s41598-021-97778-3